るのではないかと考えた。そこで，黄色ブドウ球菌ファゴソームと結核菌ファゴソームにおけるRab GTPaseの局在を網羅的に比較した[15]。黄色ブドウ球菌ファゴソームには22のRab GTPaseが局在するが，そのうちの17遺伝子が結核菌ファゴソームからかい離する，もしくは局在しないことを明らかにした。次にファゴソーム成熟に関与するRab GTPaseを同定するために，ファゴソームの酸性化とカテプシンDの局在化における不活性化型Rab遺伝子の効果を調べた。

その結果，ファゴソームの酸性化にはRab7，Rab20，Rab39が関与すること，ファゴソームへのカテプシンDの局在化にはRab7，Rab20，Rab32，Rab34，Rab38が関与することを明らかにした。これまでに，Rab7はファゴソームの酸性化とカテプシンDの局在化に関与することが明らかになっていた。Rab20は小胞体に局在するRab GTPaseであり，ファゴソーム成熟における機能は明らかになっていなかった。Rab39の局在はリソソームであり，Rab39のファゴソームへの局在は貪食後期に起こる。このことから，Rab39は貪食後期におけるファゴソームの酸性化に機能していることが示唆される。Rab32，Rab34，Rab38はトランスゴルジ網(**TGN**)に局在する[7]。

また，カテプシンDのファゴソームへの輸送は後期エンドソームやリソソームの他にもTGNから直接輸送されていることが知られている[16]。このことから，TGNから結核菌ファゴソームへのカテプシンDの輸送を阻害するため，これらのRab GTPaseが結核菌ファゴソームから排除されているのではないかと考えられる(**図2**)。

以上の結果を総合すると，結核菌はファゴソーム内のpH低下を阻害することによってカテプシンDなどの加水分解酵素をファゴソーム内で活性化させない，さらに後期エンドソーム，リソソーム，小胞体，TGNからのカテプシンDの結核菌ファゴソームへの輸送を阻害することによって結核菌ファゴソームでの殺菌因子の産生を回避していることを示唆する。

V 結核菌ファゴソームにおけるリソソームマーカーの局在

前述のように，結核菌ファゴソームでは酸性化やカテプシンDの局在化は阻害される。しかし，本当に結核菌ファゴソームはリソソームとまったく融合していないのであろうか。LAMP1やLAMP2，CD63などの古典的リソソームマーカーの局在はどうであろうか。これまで，結核菌ファゴソームには古典的リソソームマーカーが局在しないことから，結核菌ファゴソームではファゴリソソーム形成が阻害されていると主張されてきた[17]。

しかし，近年，これらの古典的マーカーが結核菌ファゴソームに局在していることが報告されている。van der Wel等はクライオ電子顕微鏡法によってLAMP1/2やCD63が結核菌ファゴソームに局在することを示した[2]。Lee等は生化学的に単離した結核菌ファゴソームのプロテオミクスによって，これらの古典的リソソームマーカーが局在することを明らかにした[18]。また，我々もイメージ解析によって結核菌ファゴソームにはこれらのリソソームマーカーが局在することを示した[12]。ノックアウトマウスの研究結果はLAMP1/2のファゴソームへの局在ヒエラルキーはRab7よりも上位にあることを示している[19]。

これらの結果は，古典的リソソームマーカーは結核菌ファゴソームでのリソソームマーカーとして機能しないことを示す。

VI おわりに

結核菌の細胞内寄生戦略におけるファゴソーム成熟阻害機構について述べた。ファゴソーム成熟を阻害する決定的な結核菌因子がいまだ見つかっていないことは，多数の結核菌因子によって協調的にファゴソーム成熟を阻害していることを示唆する。我々が明らかにしたさまざまなRab GTPaseの局在変化を指標にして，結核菌変異株ライブラリーからスクリーニングすることによってファゴ

TGN（トランスゴルジ網）

ソーム成熟を阻害する新しい結核菌因子を見出すことができる。この結核菌因子は新たな結核ワクチンや治療薬の標的となることが期待できる。

文 献

1) Russell DG : *Mycobacterium tuberculosis* : here today, and here tomorrow. Nat Rev Mol Cell Biol **2** : 569-577, 2001
2) van der Wel N, et al : *M. tuberculosis* and *M. leprae* translocate from the phagolysosome to the cytosol in myeloid cells. Cell **129** : 1287-1298, 2007
3) Stamm LM, et al : *Mycobacterium marinum* escapes from phagosomes and is propelled by actin-based motility. J Exp Med **198** : 1361-1368, 2003
4) Ogawa M, et al : Escape of intracellular *Shigella* from autophagy. Science **307** : 727-731, 2005
5) Yoshikawa Y, et al : *Listeria monocytogenes* ActA-mediated escape from autophagic recognition. Nat Cell Biol **11** : 1233-1240, 2009
6) Vieira OV, et al : Phagosome maturation : aging gracefully. Biochem J **366** : 689-704, 2002
7) Schwartz SL, et al : Wandinger-Ness A : Rab GTPases at a glance. J Cell Sci **120** : 3905-3910, 2007
8) Via LE, et al : Arrest of mycobacterial phagosome maturation is caused by a block in vesicle fusion between stages controlled by rab5 and rab7. J Biol Chem **272** : 13326-13331, 1997
9) Deretic V, et al : *Mycobacterium tuberculosis* inhibition of phagolysosome biogenesis and autophagy as a host defence mechanism. Cell Microbiol **8** : 719-727, 2006
10) Vergne I, et al : Mechanism of phagolysosome biogenesis block by viable *Mycobacterium tuberculosis*. Proc Natl Acad Sci USA **102** : 4033-4038, 2005
11) Sun J, et al : *Mycobacterium bovis* BCG disrupts the interaction of Rab7 with RILP contributing to inhibition of phagosome maturation. J Leukoc Biol **82** : 1437-1445, 2007
12) Seto S, et al : Dissection of Rab7 localization on *Mycobacterium tuberculosis* phagosome. Biochem Biophys Res Commun **387** : 272-277, 2009
13) Roberts EA, et al : Higher order Rab programming in phagolysosome biogenesis. J Cell Biol **174** : 923-929, 2006
14) Kyei GB, et al : Rab14 is critical for maintenance of *Mycobacterium tuberculosis* phagosome maturation arrest. EMBO J **25** : 5250-5259, 2006
15) Seto S, et al : Rab GTPases regulating phagosome maturation are differentially recruited to mycobacterial phagosomes. Traffic **12** : 407-420, 2011
16) Ullrich HJ, et al : Direct delivery of procathepsin D to phagosomes : implications for phagosome biogenesis and parasitism by *Mycobacterium*. Eur J Cell Biol **78** : 739-748, 1999
17) Clemens DL, Horwitz MA : Characterization of the *Mycobacterium tuberculosis* phagosome and evidence that phagosomal maturation is inhibited. J Exp Med **181** : 257-270, 1995
18) Lee BY, et al : The *Mycobacterium bovis* bacille Calmette-Guerin phagosome proteome. Mol Cell Proteomics **9** : 32-53, 2010
19) Huynh KK, et al : LAMP proteins are required for fusion of lysosomes with phagosomes. EMBO J **26** : 313-324, 2007

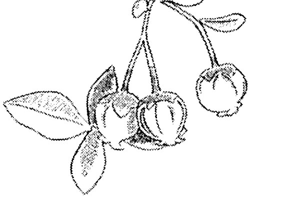

Biochemical and Biophysical Research Communications 410 (2011) 371–375

Contents lists available at ScienceDirect

Biochemical and Biophysical Research Communications

journal homepage: www.elsevier.com/locate/ybbrc

Mobility of late endosomal and lysosomal markers on phagosomes analyzed by fluorescence recovery after photobleaching

Keiko Sugaya [a], Shintaro Seto [b,*], Kunio Tsujimura [b], Yukio Koide [b,c]

[a] Department of Health Science, Hamamatsu University School of Medicine, 1-20-1 Handa-yama, Higashi-ku, Hamamatsu 431-3192, Japan
[b] Department of Infectious Diseases, Hamamatsu University School of Medicine, 1-20-1 Handa-yama, Higashi-ku, Hamamatsu 431-3192, Japan
[c] Hamamatsu University School of Medicine, 1-20-1 Handa-yama, Higashi-ku, Hamamatsu 431-3192, Japan

ARTICLE INFO

Article history:
Received 30 May 2011
Available online 12 June 2011

Keywords:
Fluorescence recovery after photobleaching
IFN-γ
LAMP1
Mycobacterium bovis BCG
Phagosome
Rab7

ABSTRACT

During phagosome maturation, the late endosomal marker Rab7 and the lysosomal marker LAMP1 localize to the phagosomes. We investigated the mobility of Rab7 and LAMP1 on the phagosomes in macrophages by fluorescence recovery after photobleaching (FRAP) analysis. Rab7 was mobile between the phagosomal membrane and the cytosol in macrophages that ingested latex beads during phagosome maturation. The addition of interferon-γ (IFN-γ) restricted this mobility, suggesting that Rab7 is forced to bind to the phagosomal membrane by IFN-γ-mediated activation. Immobilization of LAMP1 on the phagosomes was observed irrespective of IFN-γ-activation. We further examined the mobility of Rab7 on the phagosomes containing *Mycobacterium bovis* BCG by FRAP analysis. The rate of fluorescence recovery for Rab7 on mycobacterial phagosomes was lower than that on the phagosomes containing latex beads, suggesting that mycobacteria impaired the mobility of Rab7 and arrested phagosome maturation.

1. Introduction

Innate immunity provides the first line of defense against infection, and phagocytosis is an important step in the innate immune response. Pathogens phagocytosed by macrophages are enclosed into phagosomes, which interact with early and late endosomal vesicles. During this process, known as phagosome maturation, phagosomes acquire degradative and microbicidal properties and undergo phagolysosome biogenesis by fusing with lysosomes. Several proteins, including Rab GTPase proteins, play pivotal roles in phagosome maturation and phagolysosome biogenesis [1]. Rab5 is associated with early phagosomes followed by recruitment of its effector proteins, EEA1 and Class III phosphatidylinositol 3-kinase [2]. Rab7 appears on the phagosome membrane after Rab5 dissociation and resides there during phagosome maturation [3]. Rab7 regulates the transportation and fusion of late endosomes and lysosomes [1]. As an example, Rab7-interacting-lysosomal protein (RILP), an effector protein of Rab7, recruits the minus-end motor complex dynein–dynactin to the phagosome, resulting in migration of the phagosomes to the microtubule-organizing center where late endosomal and lysosomal compartments accumulate [4]. Lysosomal-associated membrane protein 1 (LAMP1) and LAMP2, the major components of lysosomes, accumulate in phagolysosomes via the fusion of lysosomes with the phagosome [5]. Although Rab7, LAMP1 and LAMP2 have important roles in the process of phagosome maturation and phagolysosome biogenesis [1,6], the accumulation kinetics of these late endosomal and lysosomal markers is not yet fully understood.

Mycobacterium tuberculosis is the causative agent of tuberculosis and has the ability to survive and replicate in macrophages. It is long believed that *M. tuberculosis* causes the arrest of phagosome maturation during Rab5–Rab7 conversion [7,8] and survives within infected macrophages. However, Sun et al. [9] reported that Rab7 localizes to the phagosomes containing *Mycobacterium bovis* BCG. We recently reported that Rab7 is transiently recruited to and subsequently released from the phagosomes containing *M. tuberculosis* using imaging and biochemical analyses [10,11]. Evidence regarding Rab7 localization to mycobacterial phagosomes is accumulating; however, detailed localization kinetics remain to be elucidated.

To understand the localization kinetics of Rab7 and LAMP1 to the phagosome membrane, we employed fluorescence recovery after photobleaching (FRAP) analysis and chased their mobility on the phagosomes in macrophages during phagosome maturation in the presence and absence of interferon (IFN)-γ. We further examine the mobility of Rab7 on the phagosomes containing *M. bovis* BCG.

2. Materials and methods

2.1. Cell and bacterial cultures

Raw264.7 macrophages were obtained from the American Type Culture Collection and maintained in Dulbecco's modified Eagle's medium (DMEM) supplemented with 10% foetal bovine serum

* Corresponding author. Fax: +81 53 435 2335.
E-mail address: s-seto@hama-med.ac.jp (S. Seto).

0006-291X/$ - see front matter
doi:10.1016/j.bbrc.2011.06.023

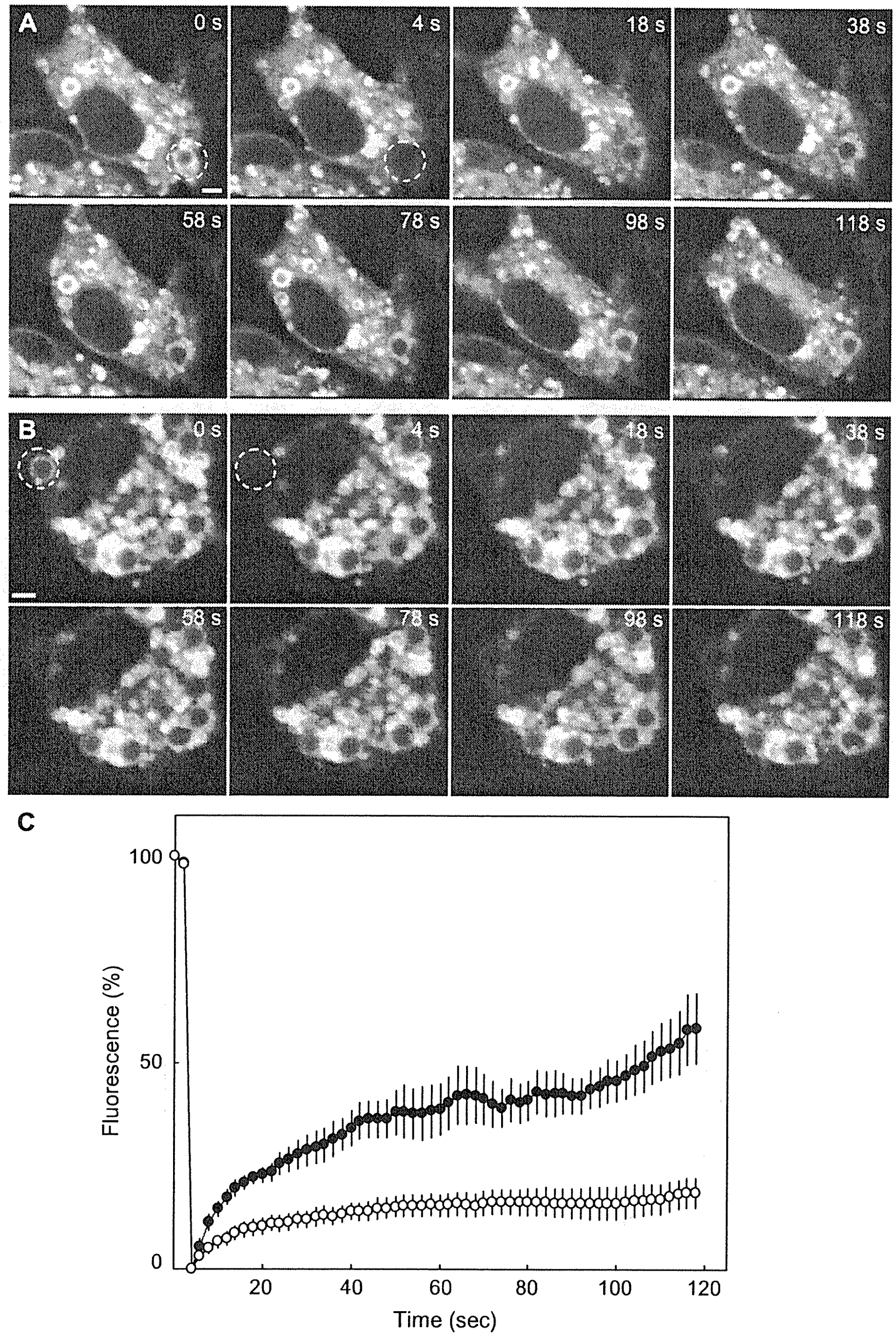

Fig. 1. FRAP analysis of EGFP-Rab7 on phagosomes. (A and B) Representative sequences of images from FRAP analysis of EGFP-Rab7 on phagosomes containing latex beads with (A) or without (B) IFN-γ stimulation. The regions marked by broken-line circles were photobleached for 4 s, and the recovery of fluorescence was monitored. (C) Temporal changes in fluorescence intensity on the bleached phagosomes. The relative intensity was defined as the ratio of fluorescence intensity at each time point to that at 0 s. The value zero was defined as the value obtained just after photobleaching. Closed and open circles indicate the relative intensities with (n = 13) or without (n = 14) IFN-γ stimulation, respectively. Data represent means and standard errors of means (SEM).

(FBS), 25 μg/ml penicillin G, and 25 μg/ml streptomycin at 37 °C under 5% CO_2. *M. bovis* BCG Tokyo transformed with a plasmid expressing DsRed [12] was grown to mid-logarithmic phase in 7H9 medium supplemented with 10% Middlebrook ADC (BD Biosciences), 0.5% glycerol and 0.05% Tween 80 containing 25 μg/ml kanamycin at 37 °C.

2.2. Plasmid constructs and transfection

Construction of the plasmid expressing enhanced green fluorescent protein (EGFP)-Rab7 has been previously described [10]. Human LAMP1 was amplified by PCR using cDNA derived from HeLa cells as a template, and the following primers: 5′-CTCGAGCCACCATGGCGGCCCCCGGCAGCGC-3′ and 5′-GGATCCCGATAGTCTGGTAGCCTGCGTGACTCCTC-3′. The PCR product corresponding to LAMP1 was inserted into pEGFP-N2 (Clontech). Transfection of cells was performed as described previously [10,11,13]. Briefly, 1×10^6 Raw264.7 macrophages were transfected with 10 μg of plasmid DNA using an MP-100 electroporator (Digital Bio Technology), according to the manufacturer's instructions. Transfected cells were grown in DMEM with 10% FBS for 24 h prior to the experiments. Transfected cells were incubated with murine IFN-γ

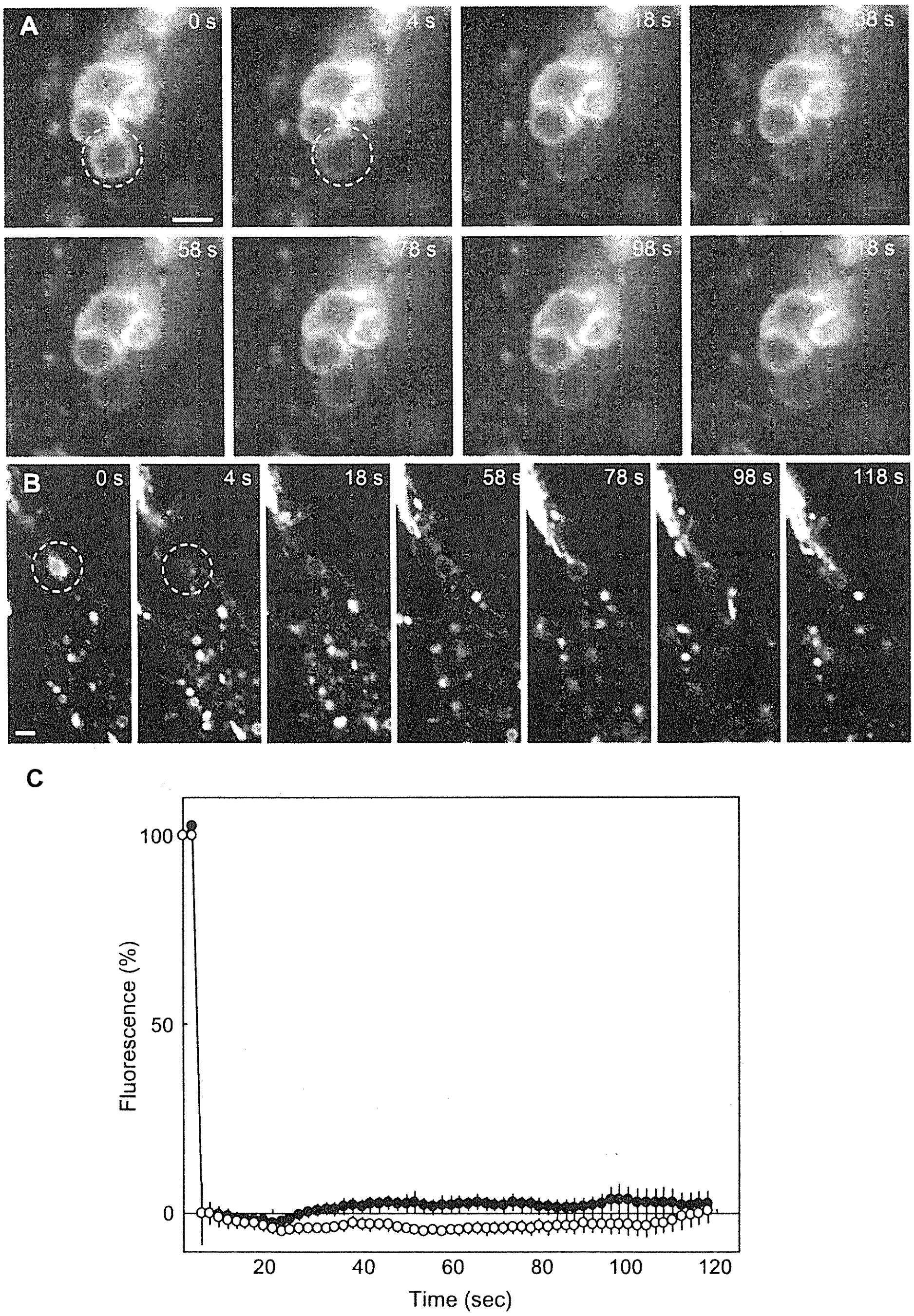

Fig. 2. FRAP analysis of LAMP1-EGFP on phagosomes. (A and B) Representative sequences of images from FRAP analysis of LAMP1-EGFP on phagosomes containing latex beads with (A) or without (B) IFN-γ stimulation. The regions marked by broken-line circles were photobleached for 4 s, and the recovery of fluorescence monitored. (C) Temporal changes in fluorescence intensity of bleached phagosomes. The relative intensity was defied as the ratio of intensity at each time point to that at 0 s. The value zero was defined as the value obtained just after photobleaching. Closed and open circles indicate the fluorescence intensities with (n = 14) or without (n = 13) IFN-γ stimulation, respectively. Data represent means and SEM.

(PeproTech, Inc.) at 10 ng/ml for 12 h before phagocytosis to activate the cells when required.

2.3. FRAP analysis

FRAP analysis was performed using an FV1000-D confocal microscope (Olympus) with a 60×/1.4 numerical aperture oil-immersion objective lens. Transfected cells (3×10^5 cells) grown on 35-mm glass dishes were allowed to phagocytose latex beads or *M. bovis* BCG expressing DsRed at 10–30 multiplicity of infection. Synchronous phagocytosis or infection was performed by centrifugation, washing with DMEM, and incubating with DMEM containing 10% FBS and 20 mM HEPES (pH 7.3) without phenol red. Temperature regulation of cells was carried out using an ONICS incubation system (Tokai Hit). The area of the phagosome surrounded by EGFP-Rab7 or LAMP1-EGFP was photobleached using a 410-nm laser at 15–20% power for 300 ms after pre-bleached images were acquired. Following photobleaching, the recovery of fluorescence was monitored at every 2 s using a 488-nm laser at 1–2% power for the phagosomes containing latex

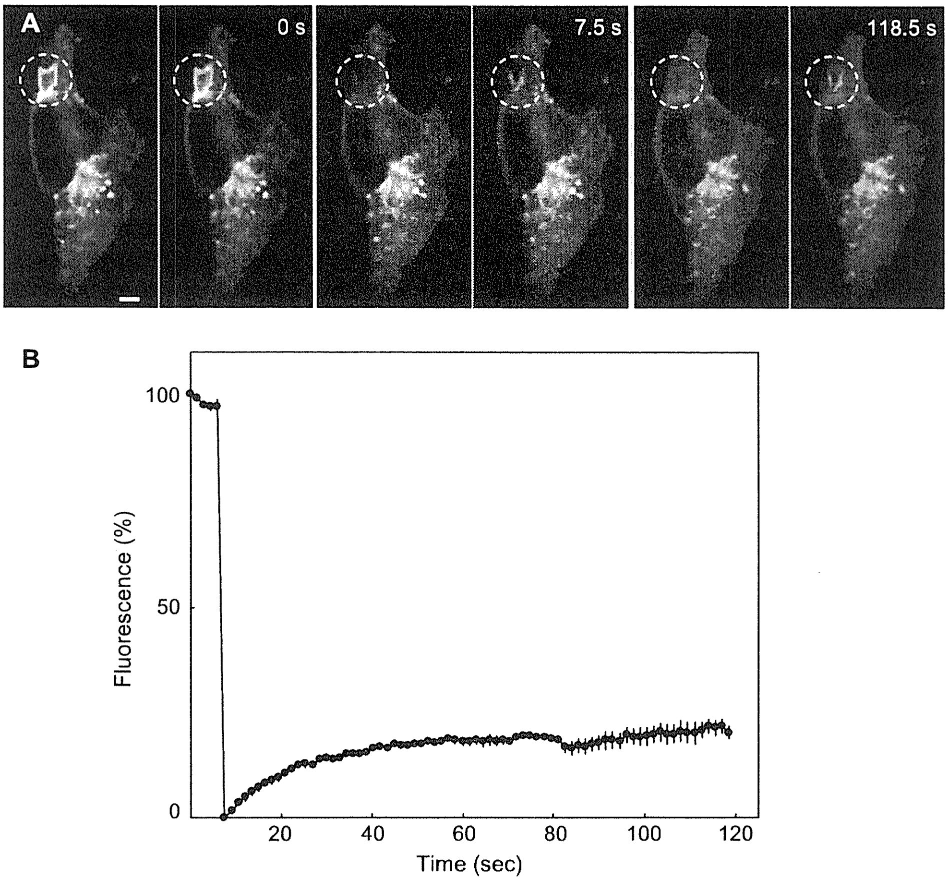

Fig. 3. FRAP analysis of EGFP-Rab7 on mycobacterial phagosomes. (A) A representative sequence of images from FRAP analysis of EGFP-Rab7 on a phagosome containing *M. bovis* BCG. Left and right panels at each time point show images of the macrophages expressing EGFP-Rab7 without and with images of infected *M. bovis* BCG expressing DsRed, respectively. The region marked by broken-line circles was photobleached for 6 s, and the recovery of fluorescence was monitored. (B) Temporal changes in fluorescence intensity of bleached phagosomes. The relative intensity was defined as the ratio of intensity at each time point to that at 0 s. The value zero was defined as the value obtained just after photobleaching. Data represent means and SEM ($n = 7$).

beads. For the measurement of fluorescence of phagosomes containing *M. bovis* BCG, the fluorescence recovery was measured at every 1.5 s using 488-nm and 543-nm lasers at 1–2% power. Fluorescence intensities were quantified using the ImageJ (http://rsb.info.nih.gp/ij/).

2.4. Statistics

The unpaired two-sided Student's *t*-test was used to assess the statistical significance of differences between the two groups.

3. Results and discussion

3.1. Mobility of Rab7 on phagosomes containing latex beads

To assess the mobility of Rab7, we conducted FRAP analysis on phagosomes containing latex beads in macrophages expressing EGFP-Rab7. Raw264.7 macrophages were transfected with a plasmid encoding EGFP-Rab7 and exposed to latex beads for 10 min, followed by phagosome maturation for 2 h. Phagosomes surrounded by EGFP-Rab7 were photobleached and the rate of recovery of fluorescence was monitored over time. A representative sequence of FRAP analysis is illustrated in Fig. 1A and Movie 1. After the phagosome with EGFP-Rab7 was photobleached (time: 4 s), fluorescence recovered rapidly. Quantitative analysis demonstrated that photobleached phagosomes recovered their fluorescence to 53% of the original level and the recovery half-time was 28 s (Fig. 1C). These results reflect the continuous conversion of Rab7 between GDP- and GTP-bound forms during phagosome maturation [14].

3.2. Mobility of Rab7 on the phagosomes in macrophages activated by IFN-γ

Next, we examined the mobility of Rab7 on phagosomes in macrophages activated by IFN-γ. Proteomic analysis revealed that IFN-γ influences the membrane trafficking on phagosomes containing latex beads and stimulates the accumulation of Rab7 to phagosomes [15]. However, the detailed kinetics of Rab7 localization on phagosomes in IFN-γ-activated macrophages has not been examined. Macrophages expressing EGFP-Rab7 were activated by IFN-γ for 12 h and allowed to phagocytose latex beads, with FRAP analysis performed 2 h after phagocytosis. As shown in Fig. 1B and Movie 2, after the phagosome was photobleached for 4 s, the fluorescence was very weak, even after 118 s. Quantitative analysis demonstrated that photobleached phagosomes recovered their fluorescence to 24% of the original level and the recovery half-time was 26 s (Fig. 1C). Previous reports demonstrated that the recovery of fluorescence was impaired in macrophages expressing the constitutive active form of Rab7 fused with GFP [16,17]. These results suggest that IFN-γ activates Rab7 on the phagosomes and consequently limits the conversion from its GTP- to GDP-bound form.

3.3. Mobility of LAMP1 on the phagosomes

To chase the mobility of LAMP1 on phagosomes, we conducted FRAP analysis on phagosomes in Raw264.7 macrophages expressing

LAMP1-EGFP. Macrophages transfected with LAMP1-EGFP were allowed to phagocytose latex beads; this was then followed by phagosome maturation for 2 h. Phagosomes surrounded by LAMP1-EGFP were photobleached and the recovery rate of fluorescence was monitored over time. As shown in Fig. 2A and Movie 3, the recovery of fluorescence was very weak, even after 118 s. Quantitative analysis revealed that the recovery rate of fluorescence was 19% of the original level and the recovery half-time for fluorescence was 42 s (Fig. 2C). FRAP analysis on phagosomes surrounded by LAMP1-EGFP in macrophages activated by IFN-γ revealed that addition of IFN-γ did not affect LAMP1 trafficking to the phagosomes (Fig. 2B and C and Mov. 4). These results suggest that LAMP1 is not directly sorted from the trans-Golgi network [18], but recruited by the fusion of lysosomal vesicles to the phagosomes.

3.4. Mobility of Rab7 on mycobacterial phagosomes

The localization of Rab7 on mycobacterial phagosomes has long been a controversial issue. Via et al. [19] first demonstrated that Rab7 does not localize to mycobacterial phagosomes, and this concept had been widely accepted [8,20]. However, Sun et al. [9] reported that Rab7 localizes to phagosomes containing *M. bovis* BCG. We also recently reported that Rab7 is transiently recruited to and subsequently released from phagosomes containing *M. tuberculosis* [10,11]. Besides localization, changes in the mobility of Rab7 on mycobacterial phagosomes have not been examined. In this study, we carried out FRAP analysis on Rab7-positive phagosomes containing *M. bovis* BCG (Fig. 3). Fig. 3A and Movie 5 illustrates a representative sequence from FRAP analysis of a mycobacterial phagosome. The mycobacterial phagosome surrounded by EGFP-Rab7 was photobleached at 6 s. The recovery of fluorescence by the mycobacterial phagosome was very weak 118.5 s after photobleaching, in contrast to that in phagosomes with latex beads (Fig. 1A). Quantitative analysis revealed that only 29% recovery was achieved and fluorescence recovery half-time was 25 s, suggesting that Rab7 is trapped in mycobacterial phagosomes. Previous reports demonstrated that RILP does not localize to mycobacterial phagosomes despite Rab7 localization [9,13]. The mobility of Rab7 is also restricted to the phagosomes containing *Salmonella* and *Burkholderia*, while RILP does not localize to these phagosomes despite Rab7 localization [16,17]. These results imply that mycobacteria may affect the activation state of Rab7 on phagosomes. Alternatively, mycobacterial phagosomes may acquire the ability to actively refuse the binding of Rab7, because the proportion of Rab7-positive mycobacterial phagosomes increases initially, then decreases 1 h after phagocytosis [10,11].

Acknowledgments

We thank Drs. Toshi Nagata and Masato Uchijima (Hamamatsu University School of Medicine, Hamamatsu, Japan) for their helpful discussions. We also thank Ms Yumiko Suzuki (Hamamatsu University School of Medicine) for her excellent assistance. This work was supported in part by Grants-in-Aid for Young Scientists (B), Scientific Research (B) and Scientific Research (C) from the Japan Society for the Promotion of Science; Scientific Research on Priority Areas from the Ministry of Education, Culture, Sports, Science and Technology of Japan; the Health and Labour Science Research Grants for Research into Emerging and Reemerging Infectious Diseases from the Ministry of Health, Labour and Welfare of Japan; and the United States-Japan Cooperative Medical Science Committee.

Appendix A. Supplementary data

Supplementary data associated with this article can be found, in the online version, at doi:10.1016/j.bbrc.2011.06.023.

References

[1] O.V. Vieira, R.J. Botelho, S. Grinstein, Phagosome maturation: aging gracefully, Biochem. J. 366 (2002) 689–704.
[2] O.V. Vieira, R.J. Botelho, L. Rameh, S.M. Brachmann, T. Matsuo, H.W. Davidson, A. Schreiber, J.M. Backer, L.C. Cantley, S. Grinstein, Distinct roles of class I and class III phosphatidylinositol 3-kinases in phagosome formation and maturation, J. Cell. Biol. 155 (2001) 19–25.
[3] O.V. Vieira, C. Bucci, R.E. Harrison, W.S. Trimble, L. Lanzetti, J. Gruenberg, A.D. Schreiber, P.D. Stahl, S. Grinstein, Modulation of Rab5 and Rab7 recruitment to phagosomes by phosphatidylinositol 3-kinase, Mol. Cell. Biol. 23 (2003) 2501–2514.
[4] R.E. Harrison, C. Bucci, O.V. Vieira, T.A. Schroer, S. Grinstein, Phagosomes fuse with late endosomes and/or lysosomes by extension of membrane protrusions along microtubules: role of Rab7 and RILP, Mol. Cell. Biol. 23 (2003) 6494–6506.
[5] E.L. Eskelinen, Y. Tanaka, P. Saftig, At the acidic edge: emerging functions for lysosomal membrane proteins, Trends Cell. Biol. 13 (2003) 137–145.
[6] K.K. Huynh, E.L. Eskelinen, C.C. Scott, A. Malevanets, P. Saftig, S. Grinstein, LAMP proteins are required for fusion of lysosomes with phagosomes, EMBO J. 26 (2007) 313–324.
[7] J. Rink, E. Ghigo, Y. Kalaidzidis, M. Zerial, Rab conversion as a mechanism of progression from early to late endosomes, Cell 122 (2005) 735–749.
[8] I. Vergne, J. Chua, S.B. Singh, V. Deretic, Cell biology of *Mycobacterium tuberculosis* phagosome, Annu. Rev. Cell. Dev. Biol. 20 (2004) 367–394.
[9] J. Sun, A.E. Deghmane, H. Soualhine, T. Hong, C. Bucci, A. Solodkin, Z. Hmama, *Mycobacterium bovis* BCG disrupts the interaction of Rab7 with RILP contributing to inhibition of phagosome maturation, J. Leukoc. Biol. 82 (2007) 1437–1445.
[10] S. Seto, S. Matsumoto, I. Ohta, K. Tsujimura, Y. Koide, Dissection of Rab7 localization on *Mycobacterium tuberculosis* phagosome, Biochem. Biophys. Res. Commun. 387 (2009) 272–277.
[11] S. Seto, K. Tsujimura, Y. Koide, Rab GTPases regulating phagosome maturation are differentially recruited to mycobacterial phagosomes, Traffic 12 (2011) 407–420.
[12] K. Aoki, S. Matsumoto, Y. Hirayama, T. Wada, Y. Ozeki, M. Niki, P. Domenech, K. Umemori, S. Yamamoto, A. Mineda, M. Matsumoto, K. Kobayashi, Extracellular mycobacterial DNA-binding protein 1 participates in mycobacterium-lung epithelial cell interaction through hyaluronic acid, J. Biol. Chem. 279 (2004) 39798–39806.
[13] S. Seto, S. Matsumoto, K. Tsujimura, Y. Koide, Differential recruitment of CD63 and Rab7-interacting-lysosomal-protein to phagosomes containing *Mycobacterium tuberculosis* in macrophages, Microbiol. Immunol. 54 (2010) 170–174.
[14] J.H. Brumell, M.A. Scidmore, Manipulation of rab GTPase function by intracellular bacterial pathogens, Microbiol. Mol. Biol. Rev. 71 (2007) 636–652.
[15] I. Jutras, M. Houde, N. Currier, J. Boulais, S. Duclos, S. LaBoissiere, E. Bonneil, P. Kearney, P. Thibault, E. Paramithiotis, P. Hugo, M. Desjardins, Modulation of the phagosome proteome by interferon-gamma, Mol. Cell Proteomics 7 (2008) 697–715.
[16] R.E. Harrison, J.H. Brumell, A. Khandani, C. Bucci, C.C. Scott, X. Jiang, B.B. Finlay, S. Grinstein, *Salmonella* impairs RILP recruitment to Rab7 during maturation of invasion vacuoles, Mol. Biol. Cell. 15 (2004) 3146–3154.
[17] K.K. Huynh, J.D. Plumb, G.P. Downey, M.A. Valvano, S. Grinstein, Inactivation of macrophage Rab7 by *Burkholderia cenocepacia*, J. Innate Immun. 2 (2010) 522–533.
[18] N.R. Cook, P.E. Row, H.W. Davidson, Lysosome associated membrane protein 1 (Lamp1) traffics directly from the TGN to early endosomes, Traffic 5 (2004) 685–699.
[19] L.E. Via, D. Deretic, R.J. Ulmer, N.S. Hibler, L.A. Huber, V. Deretic, Arrest of mycobacterial phagosome maturation is caused by a block in vesicle fusion between stages controlled by rab5 and rab7, J. Biol. Chem. 272 (1997) 13326–13331.
[20] V. Deretic, I. Vergne, J. Chua, S. Master, S.B. Singh, J.A. Fazio, G. Kyei, Endosomal membrane traffic: convergence point targeted by *Mycobacterium tuberculosis* and HIV, Cell. Microbiol. 6 (2004) 999–1009.

Cancer Immunol Immunother
DOI 10.1007/s00262-011-1015-5

ORIGINAL ARTICLE

Enhanced anti-tumor immunity by superantigen-pulsed dendritic cells

Masato Kato · Yutaro Nakamura · Takafumi Suda · Yuichi Ozawa · Naoki Inui · Naohiro Seo · Toshi Nagata · Yukio Koide · Pawel Kalinski · Hirotoshi Nakamura · Kingo Chida

Received: 24 August 2010 / Accepted: 31 March 2011

Abstract Staphylococcal enterotoxins A (SEA) and B (SEB) are classical models of superantigens (SAg), which induce potent T-cell-stimulating activity by forming complexes with MHC class II molecules on antigen-presenting cells. This large-scale activation of T-cells is accompanied by increased production of cytokines such as interferon-γ (IFN-γ). Additionally, as we previously reported, IFN-γ-producing CD8$^+$ T cells act as "helper cells," supporting the ability of dendritic cells to produce interleukin-12 (IL-12)p70. Here, we show that DC pulsed with SAg promote the enhancement of anti-tumor immunity. Murine bone marrow-derived dendritic cells (DC) were pulsed with OVA$_{257-264}$ (SIINFEKL), which is an H-2Kb target epitope of EG7 [ovalbumin (OVA)-expressing EL4] cell lines, in the presence of SEA and SEB and were subcutaneously injected into naïve C57BL/6 mice. SAg plus OVA$_{257-264}$-pulsed DC vaccine strongly enhanced peptide-specific CD8$^+$ T cells exhibiting OVA$_{257-264}$-specific cytotoxic activity and IFN-γ production, leading to the induction of protective immunity against EG7 tumors. Furthermore, cyclophosphamide (CY) added to SAg plus tumor-antigens (OVA$_{257-264}$, tumor lysate, or TRP-2) pulsed DC immunization markedly enhanced tumor-specific T-cell expansion and had a significant therapeutic effect against various tumors (EG7, 2LL, and B16). Superantigens are potential candidates for enhancing tumor immunity in DC vaccines.

Keywords Superantigen · Dendritic cell · Low-dose cyclophosphamide · Cancer vaccine · Cellular immunotherapy

Introduction

Staphylococcal enterotoxins A (SEA) and B (SEB) are classical models of bacterial superantigens (SAg). Unlike conventional antigens, SAg bind directly to the lateral surfaces of MHC class II molecules and to the Vβ domain of the TCR; therefore, they do not need to be processed and presented like conventional antigens [1–4]. This ability enables SAg to induce large-scale activation of the immune system by stimulating the large number of T-cells that express β-chains of the T-cell antigen receptor, which contain variable regions coded for by specific families of Vβ genes. Furthermore, this large-scale activation of T-cells is accompanied by the increased production of tumoricidal cytokines such as interferon-γ (IFN-γ) [5–7], although a

M. Kato · Y. Nakamura (✉) · T. Suda · Y. Ozawa · N. Inui · H. Nakamura · K. Chida
Second Division, Department of Internal Medicine, Hamamatsu University School of Medicine, 1-20-1 Handayama, Hamamatsu 431-3192, Japan
e-mail: nakayuta@hama-med.ac.jp

N. Inui
Department of Clinical Pharmacology and Therapeutics, Hamamatsu University School of Medicine, Hamamatsu, Japan

N. Seo
Department of Dermatology, Hamamatsu University School of Medicine, Hamamatsu, Japan

T. Nagata
Department of Health Science, Hamamatsu University School of Medicine, Hamamatsu, Japan

Y. Koide
Department of Infectious Diseases, Hamamatsu University School of Medicine, Hamamatsu, Japan

P. Kalinski
Department of Surgery, Immunology, Infectious Diseases and Microbiology, University of Pittsburgh, Pittsburgh, PA, USA

Published online: 26 April 2011

majority of the expanding cells will subsequently be deleted by the induction of apoptosis, and the remaining CD4$^+$ T cells will become anergic upon subsequent exposure to the SAg [8–10].

DC are specialized APC, which exist in virtually every tissue, capture antigens in situ, and migrate to lymphoid organs to activate naive T cells. DC are able to bind to much higher levels of SAg than other APC, and very small numbers of superantigen-MHC class II complexes are sufficient to trigger resting primary T cells [11, 12]. Recently, it became apparent that CD8$^+$ T cells can also activate DC and support type-1 immunity as well as CD4$^+$ T cells [13–15]. This "helper" function of CD8$^+$ T cells depends on their ability to produce IFN-γ and to promote the dendritic cell production of interleukin-12 (IL-12) p70, the key factor supporting T helper 1 responses and CTL responses [16].

DC-based tumor vaccines have demonstrated effective antitumor immune responses in vitro and after adoptive transfer in mice and humans. However, difficulties still remain to be overcome when they are used clinically [17, 18]. We evaluated the capacity of SAg to enhance DC vaccines in the setting of some tumors including poorly immunogenic B16 melanoma. We demonstrate here that simultaneous pulsing of DC with SAg and tumor antigen results in pronounced enhancement of vaccine-mediated immune priming. Furthermore, tumor antigen and SAg-pulsed DC are capable of significantly suppressing the growth of established tumors and inducing a strong antitumor T-cell response after pretreatment with cyclophosphamide (CY) in a therapeutic setting [19].

Materials and methods

Mice

Six to 8-week-old male C57BL/6 mice purchased from Japan SLC, Inc. and C57BL/6-IL12^{tmljm} (p40-knockout) mice purchased from the Jackson Laboratory were maintained in microisolator cages and used for all experiments at 8–10 weeks of age. All experimental procedures were approved by our institutional Animal Care and Use Committee.

Cell line, cell isolation, and culture

Lewis Lung Carcinoma cells (2LL), EG7 [ovalbumin(OVA)-expressing EL4] murine lymphoma, B16-F10 murine melanoma, and J774 cells were purchased from the American Type Culture Collection. Spleen CD8$^+$ T cells were negatively selected using MACS columns (Miltenyi Biotech) with 90% to 95% purity. L^{CD40L} cells expressing CD40L on their cell surface and derived from murine Langerhans cells were kindly provided by Dr. Seo (Hamamatsu University, Japan) [20]. All cells were maintained in RPMI 1640 with 10% heat-inactivated fetal bovine serum (Invitrogen), glutamine, streptomycin, and penicillin (Invitrogen).

Superantigens

SEA and SEB were purchased from Toxin Technology. Naïve splenocytes from C57BL/6 mice were co-cultured with SEA or SEB or both for 3 days. The IFN-γ concentrations of the supernatants were determined by ELISA.

Dendritic cells

Bone marrow-derived dendritic cells (DC) were generated in cultures supplemented with granulocyte macrophage colony-stimulating factor and IL-4 (both 1,000 units/ml; R&D Systems), as described in our previous reports [21–23]. On day 7, CD11c$^+$ DC were isolated using anti-mouse CD11c-coated magnetic beads (Miltenyi Biotech) and were treated with lipopolysaccharide (250 ng/ml; Sigma–Aldrich) for 16 h. Then, the DC were collected and prepared for immunization.

Induction of IL-12p70

Antigen-free or SEA or SEB (SAg)-pulsed DC (2×10^4/0.2 ml per well) were first co-cultured for 48 h with CD8$^+$ T cells (3×10^5 from the spleens of wild-type mice), harvested, washed, counted, and stimulated (at 2×10^4/0.2 ml) with 5×10^4 CD40L-transfected L cells [22] for 24 h. The IL-12p70 concentrations of the supernatant fluid were determined by ELISA (R&D systems).

Tumor vaccines

To prepare the vaccine against EG7, after treatment with lipopolysaccharide (LPS), the DC were resuspended in RPMI 1640 and pulsed with the dominant H-2Kb-restricted ovalbumin (OVA) epitope, OVA$_{257-264}$ (SIINFEKL; synthesized by Invitrogen), alone or in combination with SAg or remained untreated (none). To prepare the B16-F10 vaccine, tyrosinase-related protein 2 (TRP-2) $_{180-188}$ (SVYDFFVWL; synthesized by Invitrogen) was used as a CTL-epitope instead of OVA$_{257-264}$. Pulsing with OVA$_{257-264}$ and TRP-2$_{180-188}$ was performed at a concentration of 10 μg/ml for 60 min. To prepare the 2LL vaccine, DC were loaded overnight with 2LL tumor cells lysates (freeze-thawed thrice, centrifuged, and supernatant collected), at a concentration of three tumor cell equivalents to one DC, in the presence of LPS. The SAg pulsing was performed at a concentration of 1 μg/ml for 60 min. The expression of

CD11c, MHC II, CD86, CD80, and CD40 was analyzed by flow cytometry before and after the SAg pulsing. All vaccines were washed twice and suspended in PBS (1×10^6 per 0.2 ml).

Induction of OVA-specific immune response and protective immunity against EG7 tumor

LPS-treated DC were pulsed with $OVA_{257-264}$ (5 μg per 1×10^6 DC) in the presence or absence of SAg (1 μg per 1×10^6 DC, respectively) and were washed twice and resuspended in PBS (1×10^6 in 0.2 ml). Wild-type C57BL/6 mice (12 per group) were subcutaneously vaccinated (day-28) once. Cells were then harvested from the spleens of 4 week-immunized mice (half of each group) and cultured in the presence of $OVA_{257-264}$ (10 μg per well) for 3 days. The IFN-γ concentrations of the supernatants were determined by ELISA. The remaining 4 week-immunized mice had high numbers of EG7 cells (5×10^6/mouse) inoculated into their right flank (day 0) in order to evaluate the protective immunity induced by the vaccine. Tumors were measured using vernier calipers every 3–4 days. Data are reported as the mean $\pm$ SE of tumor area (product of the largest perpendicular diameters). Furthermore, survival was recorded as the percentage of surviving animals after tumor injection and analyzed in EG7 tumor model.

CTL activity

Fourteen days after the tumor challenge, splenocytes were harvested from two animals per group. They were restimulated in vitro (8×10^6 per well) for 5 days with $OVA_{257-264}$-pulsed syngeneic splenocytes that had been treated with 50 μg/ml mitomycin C (Roche Diagnostics GmbH) beforehand (two responder cells to one stimulator cell) in the presence of 10 IU/ml recombinant human IL-2 (R&D Systems) in 24-well culture plates. After the collection of viable effector cells, various numbers of effector cells were co-cultured with J774 cells that had been pulsed with $OVA_{257-264}$, which were used as the target cells in this study, (at 1×10^4 cells/well) for 5 h. The cell-mediated cytotoxicity of $OVA_{257-264}$ peptide was measured using a lactate dehydrogenase (LDH) cytotoxicity detection kit (Roche Diagnostics). The LDH released into the medium was measured, and the specific lysis of the target cells was calculated as $100 \times$ ([experimental release]−[spontaneous release])/([maximal release]−[spontaneous release]) according to the manufacturer's instructions. Spontaneous and maximal release were determined in the presence of medium alone and 1% Triton X-100, respectively. For 2LL tumors, 2LL cells treated with mitomycin C were used for in vitro stimulation, and untreated 2LL cells were used as the target cells. For B16-F10 tumors, $TRP2_{180-188}$ peptides were used for in vitro stimulation, and B16-F10 cells were used as the target cells.

Therapeutic model of DC vaccine involving pretreatment with low-dose cyclophosphamide

Wild-type C57BL/6 mice (6 per group) had tumor cells s.c. inoculated into their right flank (EG7: 1.5×10^6, 2LL: 3×10^5, or B16-F10: 1.5×10^5 per mouse) (day 0). The mice were i.p inoculated with CY (1 mg/0.1 ml PBS, Sigma–Aldrich) or PBS on day 2 and s.c. vaccinated (1×10^6 DC) into the same flank on day 5. Tumor area was measured every 3–4 days. Tumor size was monitored for 14 days, and then the splenocytes from two animals per group were harvested for the CTL assay. Furthermore, survival was recorded as the percentage of surviving animals and analyzed. Survival was followed as described above in EG7 tumor model.

Flow cytometory

To determine the phenotype of cultured DCs, we stained them with phycoerythrin (PE)- or fluorescein isothiocyanate (FITC)-conjugated monoclonal antibodies against cell surface molecules (CD11c and MHC classII; obtained from Miltenyi Biotec, CD86, CD80, and CD40; obtained from Pharmingen) and analyzed on a flow cytometry (Beckman Coulter EPICS XL). To enumerate $OVA_{257-264}$-specific $CD8^+$ T cells, spleen cells from immunized mice were stained by PE-conjugated tetrameric H-2Kb/$OVA_{257-264}$ peptide complex (synthesized by MBL) and FITC-conjugated anti-CD8α monoclonal antibody (MBL) and analyzed on a flow cytometry (Beckman Coulter EPICS XL). Intracellular forkhead/winged helix transcription factor (Foxp3) staining was performed according to the manufacturer's instructions. Briefly, spleen cells from vaccinated tumor-bearing mice were firstly surface-labeled with FITC-conjugated anti-CD4 monoclonal antibody and allophycocyanin (APC)-conjugated anti-CD25 monoclonal antibody. Then, after fixation and permeabilization, the cells were stained with anti-Foxp3 PE (mouse regulatory T-cell staining kit; eBioscience) and analyzed on a flow cytometry (BD FACSAria™).

Statistical analysis

Data from multiple experiments were expressed as the mean $\pm$ SEM. Statistical evaluation of the differences between the experimental group means was performed by the Mann–Whitney *U* test, and time series analyses of tumor size between the experimental groups were performed by repeated measurements of ANOVA. Survival was analyzed by log-rank test on Kaplan–Meier survival curves using JMP (SAS Institute). All tests were two-sided and performed at the 0.05 significance level.

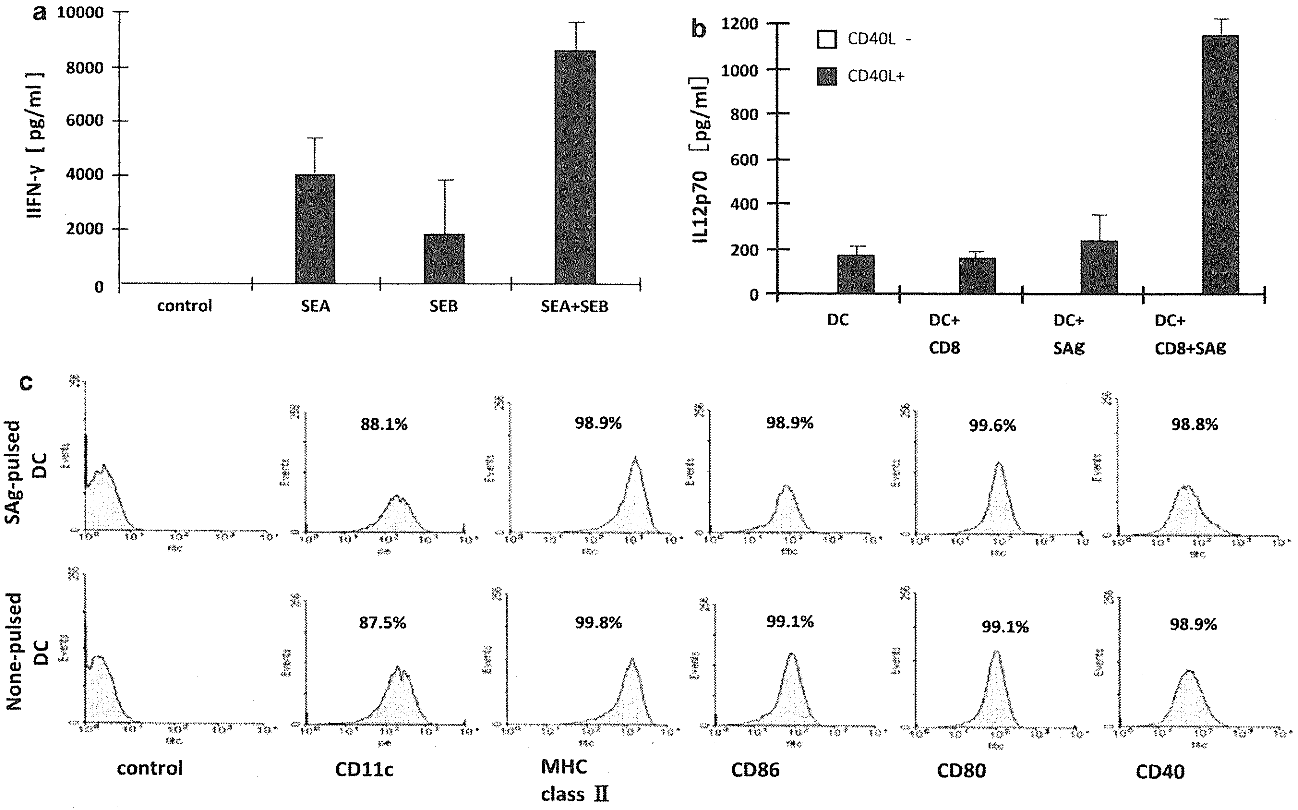

Fig. 1 DC and T-cell activation of SAg. **a** Naïve splenocytes stimulated with SEA/SEB produced significantly more IFN-γ than those stimulated with either SEA or SEB alone. Splenocytes from naïve mice were incubated in the absence or presence of SEA or SEB for 48 h. *Columns*, mean from one experiment of three that yielded similar results; *bars*, SD. **b** Interaction with $CD8^+$ T cells primes dendritic cells for high IL-12p70 production. Dendritic cells were co-cultured for 48 h with $CD8^+$ T cells from wild-type B6 mice, in the absence or presence of SEA/SEB, before being washed and stimulated with CD40L. Similar results were obtained in one additional experiment. **c** Phenotypic characteristics of SEA/SEB-pulsed DC and non-pulsed DC as determined by flow cytometry. The addition of SAg had no or a marginal effect. The expression of cell surface molecules on DC (CD11c, MHC class II, CD86, CD80, and CD40) was evaluated by flow cytometry. The data are representative of three independent experiments in which similar results were obtained

Results

Naive splenocytes strongly express IFN-γ in the presence of both SEA and SEB

To test which SAg is able to efficiently generate IFNγ-producing cells in vivo, we evaluated IFN-γ production by spleen cells from naive mice. Upon stimulation with SEA or SEB, or both, the spleen cells stimulated with a combination of SEA and SEB produced significantly higher levels of IFN-γ than spleen cells treated with either SEA or SEB (Fig. 1a).

Dendritic cell activation of $CD8^+$ T cells with SAg and their phenotype

To analyze the ability of mouse $CD8^+$ T cells to affect dendritic cell functions in vitro, we used the previously established model of SEA/SEB-driven stimulation of T cells from wild-type C57BL/6 mice. This model allowed us to promote the interaction of dendritic cells with high numbers of $CD8^+$ T cells without the need for prior T-cell activation and clonal expansion. In accordance with our previous data, freshly isolated mouse $CD8^+$ T cells primed the SEA/SEB-loaded dendritic cells for high IL-12p70 production during their subsequent interaction with CD40L-expressing L cells, which were used as $CD4^+$ T-cell surrogates (Fig. 1b).

Then, we examined the expression patterns of various cell surface molecules by flow cytometry. DC pulsed with SAg (SEA and SEB) and non-pulsed DC expressed similar amounts of CD11c, MHC class II molecules, CD86, CD80, and CD40, (Fig. 1c), indicating that pulsing SAg into DC does not affect their phenotype.

SAg/OVA-pulsed DC vaccination generates $OVA_{257-264}$-specific CTL

We determined the ability of SAg-pulsed DC to induce epitope-specific $CD8^+$ T cells in the spleen. Using an

$OVA_{257–264}$ peptide-specific H-2kb tetramer, we evaluated the frequencies of tetramer-bound $CD8^+$ T cells by flow cytometry in the spleen cells from mice that had been immunized with SAg/OVA-pulsed DC (SAg/OVA-DC) 4 week before, and compared it with that by spleen cells from mice that had been immunized with $OVA_{257–264}$-pulsed DC (OVA-DC), SAg-pulsed DC (SAg-DC), none-pulsed DC (con-DC) or PBS. Immunization with SAg/OVA-DC resulted in significantly higher numbers of $OVA_{257–264}$-specific $CD8^+$ cells than immunization with OVA-DC, SAg-DC, con-DC or PBS ($P = 0.0157$, SAg/OVA-DC vs. OVA-DC, Fig. 2a). Furthermore, upon stimulation with $OVA_{257–264}$ peptide, the spleen cells from SAg/OVA DC-immunized mice produced significantly higher levels of IFN-γ than spleen cells from mice immunized with OVA-DC, SAg-DC or con-DC (P=0.0200, SAg/OVA-DC vs. OVA-DC, Fig. 2a *inset*). Collectively, these data suggest that immunization with SAg/OVA-pulsed DC efficiently generates $OVA_{257–264}$-specific CTL and IFN-γ-producing cells in vivo.

Next, we determined the cytolytic activities of $OVA_{257–264}$-specific CTL induced by immunization with SAg/OVA-pulsed DC. After in vitro restimulation of immune spleen cells with the $OVA_{257–264}$ peptide, the cells from SAg/OVA-pulsed DC-immunized mice lysed the peptide-pulsed J774 cells more effectively than the cells from OVA-pulsed DC-immunized mice (Fig. 2b). The CTL activity of the spleen cells from the mice immunized with SAg-pulsed DC was similar to that of the spleen cells from the mice immunized with OVA-pulsed DC. These CTL activities correlated well with the frequencies of $OVA_{257–264}$-specific tetramer-bound $CD8^+$ T cells and the levels of $OVA_{257–264}$-specific IFN-γ (Fig. 2a, b).

SAg/OVA-pulsed DC vaccination provides protective immunity against a subsequent challenge with an EG7 $OVA_{257–264}$ expressing tumor

To ascertain whether the immune responses induced in the mice immunized with the DC vaccines efficiently protected against tumors, the vaccinated animals were subcutaneously challenged with EG7 tumors. The suppression of tumor growth was significantly higher in the mice that received SAg/OVA-pulsed DC than in the mice that had received OVA-pulsed DC, SAg-pulsed DC, or untreated control DC ($P = 0.0048$, SAg/OVA-DC vs. OVA-DC, Fig 2c). Subsequently, survival analysis revealed that, although all of the mice immunized with SAg-DC, OVA-DC, or control DC died within 30 days after tumor inoculation, 80% of mice immunized with SAg/OVA-pulsed DC survived (Fig. 2d). The differences in the survival curves were statistically significant between SAg/OVA-pulsed DC-immunized mice and OVA-pulsed DC-immunized mice ($P = 0.0101$).

Critical role of dendritic cells in mediating CD8 help

Whereas the inclusion of SAg strongly enhanced the immunologic and antitumor effects of vaccination in the animals, the heterologous help from $CD8^+$ T cells induced by SAg was not mediated by IL-12/IL-23-deficient dendritic cells generated from the bone marrow of p40-knockout animals (Fig. 2e, f).

SAg enhance the therapeutic efficacy of DC-based immunization against established tumors in combination with low-dose CY

To determine the therapeutic potential of immunization with SAg/OVA-pulsed DC, we attempted to induce tumor rejection in mice with EG7 tumors. In a 5-day treatment model, B6 mice harboring EG7 were treated with SAg/OVA-pulsed DC with or without low-dose CY. As shown in Fig. 3a and b, although we could not see any potential effect of this vaccine in terms of the induction of $OVA_{257–264}$-specific CTL or tumor size reduction, treatment with a combination of SAg/OVA-pulsed DC and low-dose CY markedly generated $OVA_{257–264}$-specific CTL. Furthermore, combined treatment with SAg/OVA-pulsed DC and low-dose CY resulted in a significant reduction of tumor growth ($P = 0.0015$; compared with mice receiving OVA-pulsed DC). Similar effects were observed in other two cell line two poorly immunogenic tumors (2LL and B16, respectively) (Fig. 3c–f). Collectively, these findings demonstrated that SAg enhanced the therapeutic efficacy of DC immunization and induced protective immunity against poorly immunogenic tumors, which was achieved in combination with the systemic administration of low-dose CY. Furthermore, survival analysis revealed that survival of mice vaccinated with SAg/OVA-pulsed DC were improved in EG7 model (Fig. 3g). The differences in the survival curves were statistically significant between SAg/OVA-pulsed DC-immunized mice with CY and OVA-pulsed DC-immunized mice with CY ($P = 0.0317$).

Low-dose CY support the therapeutic effect of SAg/OVA-pulsed DC vaccine by inhibiting the increase of $CD4^+CD25^+Foxp3^+$ cells

To ascertain the role of low-dose CY in the therapeutic model, the proportion of regulatory T cells of the splenocytes from vaccinated mice was investigated using flow cytometry (Fig. 4a). On day 5, after tumor inoculation, B6 mice harboring EG7 were treated with SAg/OVA-pulsed DC with or without low-dose CY. Three days after vaccination, the percentage of $CD4^+CD25^+Foxp3^+$ cells among the total $CD4^+$ cells in the spleen was increased in the tumor-bearing mice ($P = 0.0001$, Naïve vs. Tumor bearing, Fig. 4b), but was

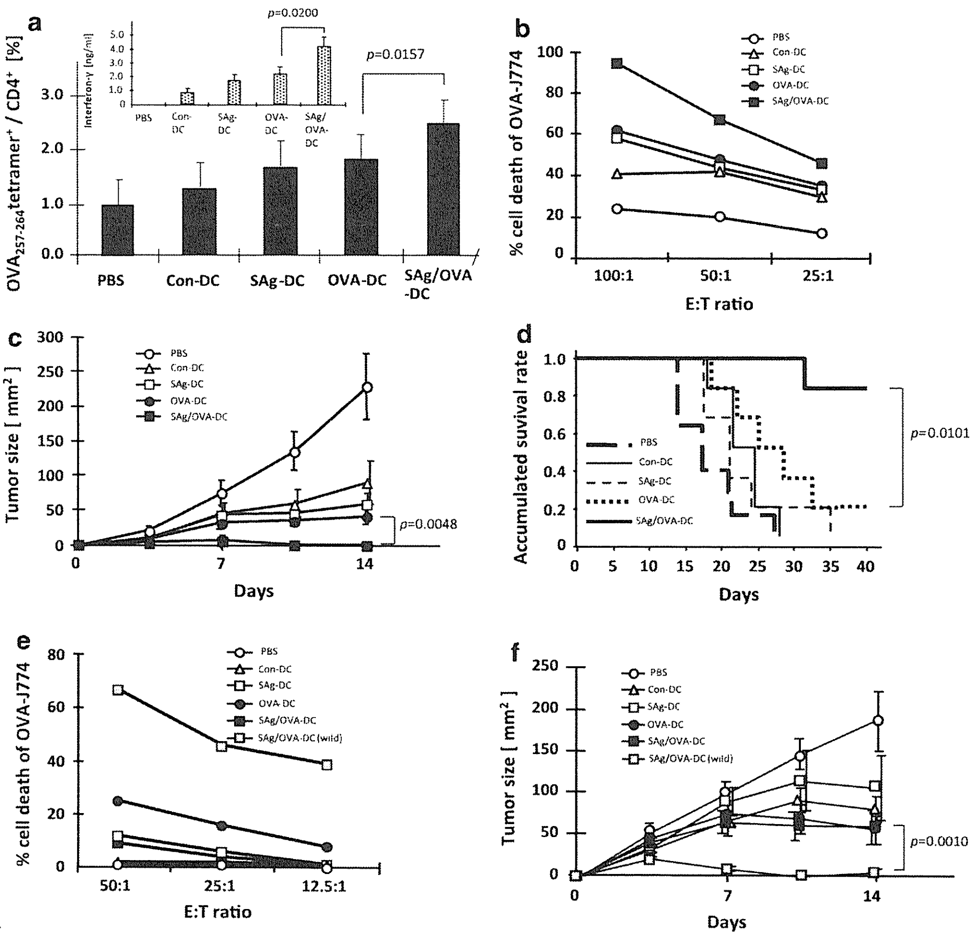

Fig. 2 SAg(SEA/SEB)-pulsed DC to induce potent anti-tumor protective immunity. **a** $OVA_{257-264}$-specific $CD8^+$ T cells in spleens of 4 week-immunized mice. Spleen cells from mice immunized with $OVA_{257-264}$ or SAg plus $OVA_{257-264}$-pulsed DC (OVA-DC and SAg/OVA-DC, respectively) or SAg-pulsed DC (SAg-DC) or none-pulsed DC (Con-DC), or from PBS immunized mice (PBS) were harvested 4 weeks after immunization and $OVA_{257-264}$-specific $CD8^+$ T cells were evaluated by flow cytometry with a tetrameric $OVA_{257-264}$ H-2kb/$OVA_{257-264}$ peptide complex. Percentage of $OVA_{257-264}$ tetramer positive cells among the total $CD8^+$ T cells was shown. The data are means and standard deviations for four mice in each experimental group. *Inset*, IFN-γ secretion by $OVA_{257-264}$-stimulated splenocytes from mice immunized with SEA/SEB plus $OVA_{257-264}$-pulsed DC or $OVA_{257-264}$-pulsed DC. The concentrations of IFN-γ in the culture supernatants were determined by a sandwich enzyme-linked immunosorbent assay. The data are means and standard deviations for six mice in each experimental group. **b** Induction of CTL specific to EG7 lymphoma. Spleen cells from mice immunized with both SAg and $OVA_{257-264}$, or either of the other pulsed DC (SAg/OVA-DC, SAg-DC, or OVA-DC) or non-pulsed DC (Con-DC), or PBS were harvested 4 weeks after immunization and stimulated in vitro with $OVA_{257-264}$ peptide-pulsed spleen cells for 5 days. The percentage of specific lysis was determined using J774 cells ($H2^d$) that had been pulsed with $OVA_{257-264}$ peptide as target cells. Immune spleen cells (effectors) were incubated with target cells at the effector-to-target-cell ratios (E/T Ratio) indicated on the *x-axis*. The data are representative of data obtained in four independent experiments. **c** Induction of protective immunity against tumor growth by immunization with SAg plus $OVA_{257-264}$ DC. The mice were immunized with the indicated vaccines. Four weeks after immunization, the mice were challenged with 1.5×10^6 of EG7 lymphoma. The data are the means and standard errors for six mice in each experimental group. **d** Survival was recorded as the percentage of surviving animals. Data represent one of two independent experiments. **e, f** IL-12p40–deficient dendritic cells (unable to produce IL-12p70 and IL-23) do not mediate heterologous CD8 help via SAg. Mice received single s.c. injections of dendritic cells (generated from wild-type or IL-12p40–knockout mice) loaded with $OVA_{257-264}$ alone or in combination with SAg. The differences between the treatment groups were evaluated by repeated measurements of ANOVA. An exact log-rank test was used to analyze the survival differences between the SAg/OVA-DC and OVA-DC treatment groups ($P = 0.0010$)

reduced by low-dose CY. Furthermore, SAg/OVA-pulsed DC vaccine induced the increase in $CD4^+CD25^+Foxp3^+$ cells and was reduced similarly by low-dose CY (P=0.0118, Tumor bearing with CY and DC vs. Tumor bearing with DC, Fig. 4b). These findings suggest that inhibition of regulatory T cells by systemic administration of low-dose CY support the therapeutic effect of SAg/OVA-pulsed DC vaccine.

Discussion

Superantigens cause intense T-cell proliferation and the production of cytokines. The predominant cytokines produced and released during superantigen activation are IL-2 and IFN-γ [5–7], both of which are intimately involved in the cytokine cascade during immune responses. One of

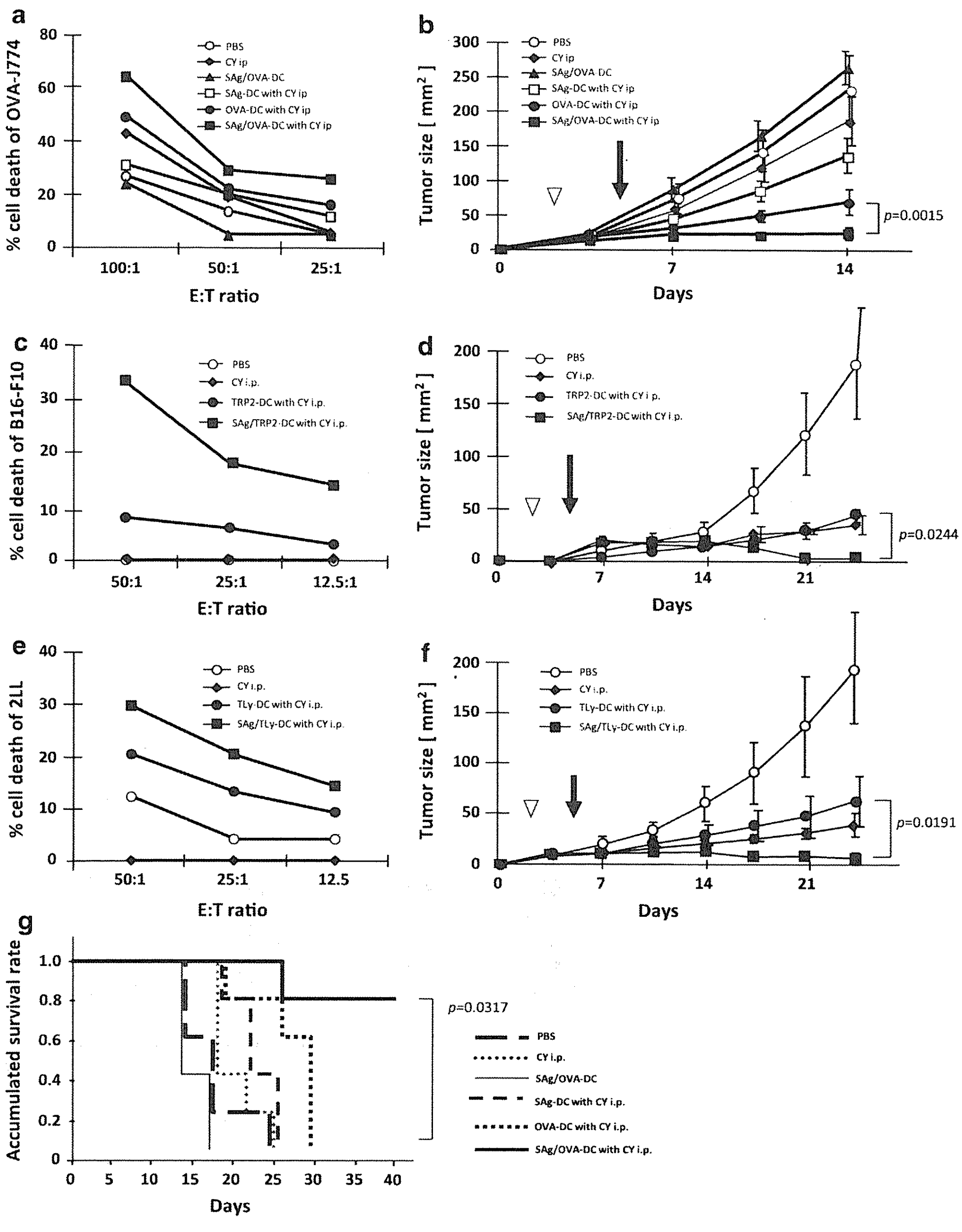

Fig. 3 SAg plus $OVA_{257-264}$-pulsed DC mediate significant therapeutic antitumor effects in combination with low-dose cyclophosphamide. **a-f** Three days after tumor inoculation, B6 mice bearing established EG7 (**a, b**), B16 (**c, d**), or 2LL (**e, f**) tumors were treated with or without cyclophosphamide followed by the indicated vaccines. **a, c, e** SAg plus $OVA_{257-264}$-pulsed DC efficiently enhance the induction of CTL specific to the individual tumors. **b, d, f** SAg with low-dose cyclophosphamide supports the therapeutic activity of cancer vaccines. The open arrowhead shows the day of CY treatment. The closed arrow shows the day of DC vaccination. Similar results were obtained in two separate experiments. Data are presented as the mean ± SE. **g** Survival of B6 mice bearing established EG7 treated with cyclophosphamide followed by the indicated vaccine was recorded as the percentage of surviving animals. An exact log-rank test was used to analyze the survival differences between the SAg/OVA-DC with CY i.p. and OVA-DC with CY i.p. treatment groups ($P = 0.0317$). Data represent one of two independent experiments

these cytokines, IFN-γ, possesses immunostimulatory activity in that it activates $CD8^+$ T cells, macrophages, and NK cells so that they become cytolytic. It was also reported that the high cytolytic activity detected in vaccinated mice given SEA/SEB was predominantly due to $CD8^+$ T cells [24]. T cells activated by superantigen promotes the maturation of DC mainly via MHC classII molecule, which contributes to induce tumor-specific CTLs [25]. Other cell types have been found to play roles in antitumor immunity, such as NK cells or activated eosinophils, which may be marginally involved. Thus, as various cancer patients have been shown to possess low levels of tumor-specific T cells, superantigens may be able to expand these small populations to produce populations that are effective at fighting the tumor.

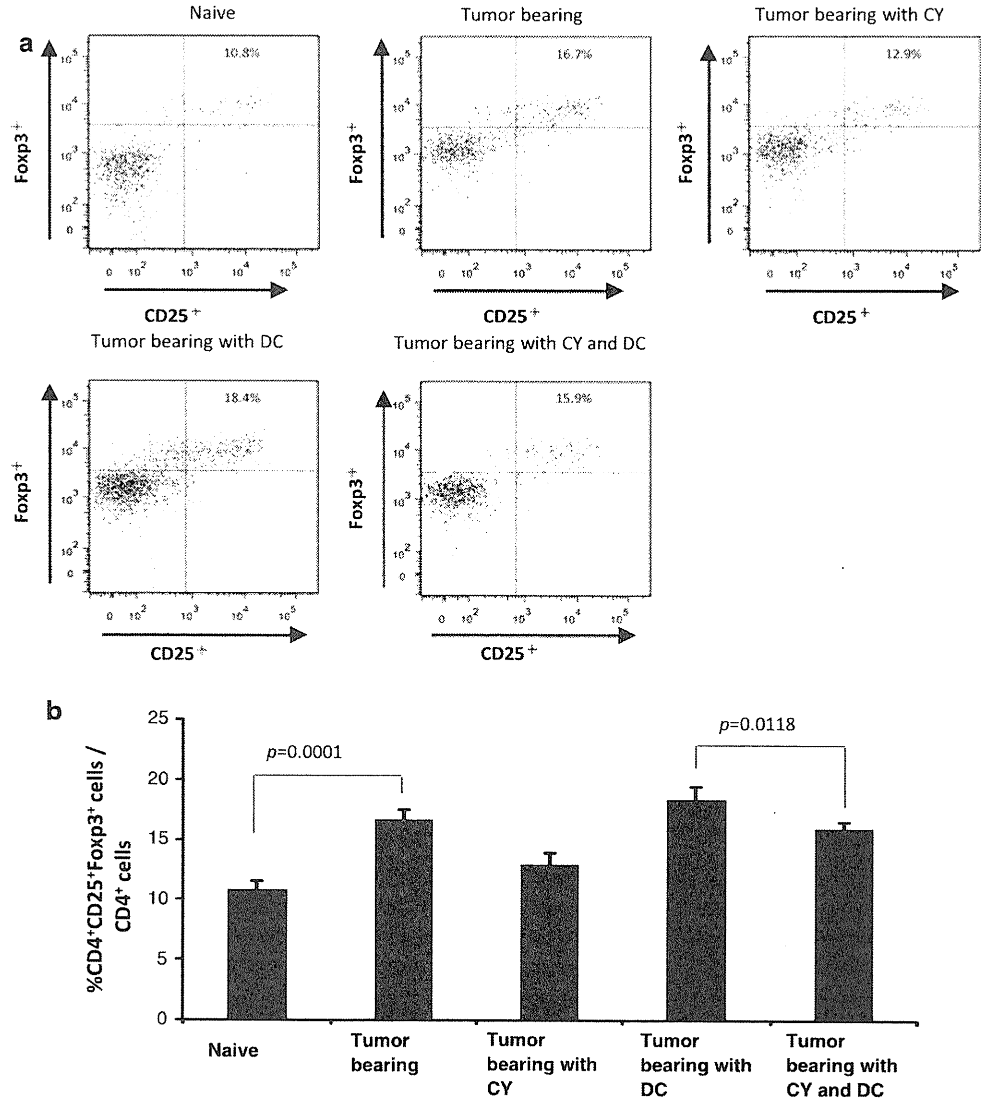

Fig. 4 CD4+CD25+Foxp3+cells (Treg) is increased in spleen of tumor-bearing mice, which is enhanced by SAg/OVA-DC vaccine but reduced by pretreatment with low-dose cyclophosphamide. As Fig. 3a, three days after tumor inoculation, B6 mice bearing established EG7 were treated with or without CY and followed by SAg/OVA-DC vaccine or PBS. On day 8 (3 days after vaccination), the spleens were harvested and analyzed by flow cytometry. **a** Representative profiles of the flow cytometry analysis. **b** Percentage of $CD4^+CD25^+Foxp3^+$ regulatory T cells among the total $CD4^+$ T cells. The data are means and standard deviations for four mice in each experimental group

IFN-γ has been shown to elicit direct anticellular effects on a variety of tumor cell lines. Furthermore, IFN-γ-induced cell growth inhibition was accompanied by the increased production of the tumor suppressor gene products p21 and p27 [26, 27]. This suggests that the direct anticellular effects of IFN-γ also contribute to the antitumor protection seen in response to vaccination followed by superantigen administration.

The ability of DC to generate potent type-1 immune responses has made them highly attractive for use as cancer vaccines where cytolytic immunity is desired for the clearance of tumor cells. IL-12 enhances natural killer cell and CTL activities and plays a key role in the induction of type-1 immune responses. Numerous studies have demonstrated that the co-administration of IL-12 or genetic engineering of DC to produce high levels of IL-12 strongly enhances the antitumor efficacy of cancer vaccines [28–30]. Recently, we found that the ability of class I restricted $CD8^+$ T cells to coactivate and polarize DC supports the induction of type-1 responses using ovalbumin or superantigen mice model [16]. Consistent with previous studies using the OVA model, heterologous help from $CD8^+$ T cells could not be mediated by IL-12/IL-23-deficient dendritic cells generated from the bone marrow of p40-knockout animals in this study, suggesting that dendritic cells play a critical role in mediating CD8 help for anticancer immunity.

Superantigenic stimulation of T cells prior to their activation by vaccination may ultimately lead to the induction of anergy [9, 10]. Furthermore, tumor-specific anergy has been shown to be an early event in the tumor-bearing host. Although the $CD4^+$ $CD25^+$ T-cell number is tightly regulated in normal conditions, they accumulate in tumor-bearing hosts [31, 32]. Valzasina et al. [32] reported $CD4^+CD25^-$ T-cell conversion into regulatory T cells (Treg) as the mechanism of Treg replenishment and expansion in tumor-bearing mice. Furthermore, therapeutic vaccination of the tumor-bearing host expanded both tumor-induced Treg and effector cells, but suppression was dominat, blunting the expansion of naïve tumor-specific T cells and blocking the execution of effector function [33]. Cyclophosphamide (CY) is an alkylating agent that is widely used in the treatment of malignancies as well as autoimmune disorders. As an immunomodulatory agent, CY increases the efficacy of various kinds of antitumor immunotherapeutic regimens, including active or adoptive immunotherapies. The administration of low-dose CY prior to DC immunization resulted in a significant increase in antitumor Th1 immune responses and a decrease in the number of $CD4^+$ $CD25^+$ Treg cells in the tumor-bearing host [34]. Our data demonstrate that although the efficacy of tumor antigen and SAg-pulsed DC was abolished in a therapeutic tumor-bearing model, significant antitumor effects were observed in animals bearing various established tumors (EG7, B16, and 2LL) after low-dose CY treatment. Complete tumor eradication was observed in 30–60% of mice treated with a single injection of SAg-pulsed DC, even when a weakly immunogenic B16 or 2LL tumor was used. Consistent with previous reports [31, 32, 34], our data also demonstrated that these efficacy might be due to an ability of CY to control the number of Treg in tumor-bearing animals.

Few studies have utilized SAg as an immune adjuvant for anti-cancer therapy. Wirth et al. [35] investigated whether the induction of a CTL response to HLA-A2-Melan-A was improved by using rVV expressing the CTL defined epitope alone or in combination with SAg. They showed that the anti-Melan-A response was efficiently induced but that tumor suppression was not significantly enhanced by coexpression of the SAg in a tumor protective model. However, the host dendritic cells might not have worked efficiently in their model. Kominsky et al. [24] reported that the vaccination of mice with irradiated B16F10 cells followed by treatment with a combination of SEA and SEB led to significant and specific protection against subsequent challenge with viable B16F10 cells. Here, we showed that tumor antigen and SAg-pulsed ex vivo generated dendritic cells efficiently induced antitumor immunity in therapeutic models (tumor-bearing state) as well as the prophylactic setting. Although SAg is known to cause toxicity through excessive immune responses, SAg was administered in several human clinical studies as well as animal studies, and no serious adverse events were reported [36–38]. Indeed, we observed five non-tumor-bearing animals that were injected with the same dose of SAg-pulsed DC, and they remained alive for at least a year.

In summary, systemic immune responses, as demonstrated by CTL activity and IFN-γ production, were significantly higher and tumor specific when SAg-pulsed DC were used. High cytolytic activity in association with a type-1 response may have contributed to the profound in vivo anti-tumor effects that we observed. These results strongly suggest that treatment with SAg-pulsed DC in combination with low-dose CY should be considered in humans, in order to facilitate the development of effective strategies for therapeutic vaccination of patients with cancer and chronic infections.

Acknowledgments We thank Drs. T. Uchiyama and H. Kato (Tokyo Women's Medical University) for providing SEA used in preliminary experiments, K. Shibata for operating flow cytometry. This work was supported by grants-in-aid for scientific research from the Japanese Society for the Promotion of Science (grant 19590889 to Y.N.).

Conflict of interest None of the authors has any financial relationships with commercial entities that have an interest in the subject of this manuscript.

References

1. White J, Herman A, Pullen AM et al (1989) The V beta-specific superantigen staphylococcal enterotoxin B: stimulation of mature T cells and clonal depetion in neonatal mice. Cell 56:27–35
2. Li H, Liera A, Tsuchiya D et al (1998) Three-dimensional structure of the complex between a T cell receptor beta chain and the superantigen staphylococcal enterotoxin B. Immunity 9:807–816
3. Malchiodi EL, Eisenstein E, Fields BA et al (1995) Superantigen binding to a T cell receptor betachain of known three-dimensional structure. J Exp Med 182:1833–1845
4. Sundberg EJ, Li H, Liera AS et al (2002) Structures of two streptococcal superantigens bound to TCR beta chains reveal diversity in the architecture of T cell signaling complexes. Structure 10:687–699
5. Kotzin BL, Leung DYM, Kappler J, Marrack P (1993) Superantigen and their potential role in human disease. Adv Immunol 54:99–166
6. Webb SR, Gascoigne NRJ (1994) T-cell activation by superantigens. Curr Opin Immunol 6:467–475
7. Litton MJ, Sander B, Murphy E et al (1994) Early expression of cytokines in lymph nodes after treatment in vivo with Staphylococcus enterotoxin B. J Immunol Methods 175:47–58
8. Kawabe Y, Ochi A (1991) Programmed cell death and extrathymic reduction of V beta8+ CD4+ T cells in mice tolerant to *Staphylococcal aureus* enterotoxin B. Nature 349:245–248
9. Heeg K, Gaus H, Griese D, Bendig S, Miethke T, Wagner H (1995) Superantigen-reactive T cells that display an anergic phenotype in vivo appear functional in vivo. Int Immunol 7:105–114
10. Sundstedt A, Dohlsten M, Hedlund G, Hoiden I, Bjorklund M, Kalland T (1994) Superantigens anergize cytokine production but not cytotoxity in vivo. Immunology 82:117–125
11. Bhardwaj N, Fried man SM, Cole BC, Nisanian AJ (1992) Cendritic cells are potent antigen-presenting cells for microbial superantigens. J Exp Med 175:267–273
12. Bhrardwaj N, Young JW, Nisanian AJ, Baggers J, Steinman RM (1993) Small amounts of superantigens, when presented on dendritic cells, are sufficient to initiatiate to T cellresponses. J Exp Med 178:633–642
13. Gurunathan S, Stobie L, Prussin C et al (2001) Requirements for the maintenance of Th1 immunity in vivo following DNAvaccination: A potential immunoregulatory role for CD8+ T cells. J Immunol 16:1283–1289
14. Wang B, Norbury CC, Greenwood R, Bonnink JR, Yewdell Jw, Frelinger JA (2001) Multiple paths for activation of naïve CD8+ T cells: CD4-independent help. J Immunol 167:1283–1289
15. Mailliard RB, Egawa S, Cai Q et al (2002) Complementary dendritic cell-activating function of CD8+ and CD4+ T cells: helper role of CD8+ T cells in the development of T helper type 1 responses. J Exp Med 195:473–483

16. Nakamura Y, Watchmaker P, Urban J et al (2007) Helper function of memory CD8+ T cells: heterologous CD8+ T cells support the induction of therapeutic cancer immunity. Cancer Res 67:10012–10018
17. Osada T, Clay TM, Woo CY, Morse MA, Lyerly HK (2006) Dendritic cell-based immunotherapy. Int Rev Immunol 25:377–413
18. Fazle Akbar SMF, Abe M, Yoshida O, Murakami H, Onji M (2006) Dendritic cell-based therapy as a multidisciplinary approach to cancer treatment: present limitations and future scopes. Curr Med Chem 13:3113–3119
19. Lutsiak MEC, Semnani RT, Pascalis RD, Kashmiri SVS, Schlom J, Sabzevari H (2005) Inhibition of CD4+25+ T regulatory cell function implicated in enhanced immune response by low-dose cyclophosphamide. Blood 105:2862–2868
20. Ito T, Seo N, Yagi H, Tsujimura K, Takigawa M, Tokura Y (2003) Alterations of immune functions in barrier disrupted skin by UVB irradiation. J Dermatol Sci 33:151–159
21. Nakamura Y, Suda T, Nagata T et al (2003) Induction of protective immunity to Listeria monocytogenes with dendritic cells retrovirally transduced with a cytotoxic T lymphocyte epitope minigene. Infect Immun 71:1748–1754
22. Enomoto N, Nagata T, Suda T et al (2007) Immunization with dendritic cells loaded with alpha-galactosylceramide at priming phase, but not at boosting phase, enhances cytotoxic T lymphocyte activity against infection by intracellular bacteria. FEMS Immunol Med Microbiol 51:350–362
23. Ozawa Y, Suda T, Nagata T et al (2009) Mucosal vaccine using CTL epitope-pulsed dendritic cells confers protection for intracellular pathogen. Am J Respir Cell Mol Biol 41:440–448
24. Kominsky SL, Torres BA, Hobeika AC, Lake FA, Johnson HM (2001) Superantigen enhanced protection against a weak tumor-specific melanoma antigen: implications for prophylactic vaccination against cancer. Int J Cancer 94:834–841
25. Muraille E, Trez DC, Pajak B, Brait M, Urbain J, Leo O (2002) T cell-dependent maturation of dendritic cells in response to bacterial superantigens. J Immunol 168:4352–4360
26. Egwu CE, Li W, Yu C-R et al (2006) Interferone-γ induce regression of epithelial cell carcinoma: critical role of IRF-1 and ICSBP transcription factors. Oncogene 25:3670–3679
27. Kortylewski M, Komyod W, Kauffmann M-E et al (2004) Interferone-γ-mediated growth regulation of melanoma cells: involvement of STAT1-dependent and STAT1-independent signals. J Invest Dermatol 122:414–422
28. He XZ, Wang L, Zhang YY (2008) An effective vaccine against colon cancer in mice: use of recombinant adenovirus interleukin-12 transduced dendritic cells. World J Gastroenterol 14:532–540
29. Iinuma H, Okinaga K, Fukushima R et al (2006) Superior protective and therapeutic effect of IL-12 and IL-18 gene-transduced dendritic neuroblastoma fusion cells on liver metastasis of murine neuroblastoma. J Immunol 176:3461–3469
30. Kim CH, Hong MJ, Park SD et al (2006) Enhancement of anti-tumor immunity specific to murine glioma by vaccination with tumor cell lysate-pulsed dendritic cells engineered to produce interleukin-12. Cancer Immunol Immunother 55:1309–1319
31. Matsushita N, Shari AP-T, Martin LM, Riker AI (2008) Comparative methodologies of regulatory T cell depletion in a murine melanoma model. J Immunol Methods 333:167–179
32. Valzasina B, Piconese S, Guiducci C, Colombo MP (2006) Tumor-induced expansion of regulatory T cells by conversion of CD4+CD25- lymphocytes is thymus and proliferation independent. Cancer Res 66:4488–4495
33. Zhou G, Drake GC, Levitsky IH (2006) Amplification of tumor-specific regulatory T cells following therapeutic cancer vaccines. Blood 107:628–636
34. Liu JY, Wu Y, Zhang XS et al (2007) Single administration of low dose cyclophosphamide augments the antitumor effect of dendritic cell vaccine. Cancer Immunol Immunother 56:1597–1604
35. Wirth S, Bille F, Koenig S et al (2002) Testing mouse mammary virus superantigen as adjuvant in cytotoxic T-lymphcyte responses against a melanoma tumor antigen. Int J Cancer 99:201–206
36. Cheng JD, Babb JS, Langer C et al (2004) Individualized patient dosing in phase I clinical trials: the role of escalation with overdose control in PNU-214936. J Clin Oncol 22:602–609
37. Fangming Xiu, Cai Z, Yang Y, Wang X, Wang J, Cao X (2007) Surface anchorage of superantigen SEA promotes induction of specific antitumor immune response by tumor-derived exosomes. J Mol Med 85:511–521
38. Ren S, Terman DS, Bohach G et al (2004) Intrapleural staphylococcal superantigen induces resolution of malignant pleural effusions and and a survival benefit in non-small cell lung cancer. Chest 125:1529–1539

Traffic 2011; **12:** 407–420

doi:10.1111/j.1600-0854.2011.01165.x

Rab GTPases Regulating Phagosome Maturation Are Differentially Recruited to Mycobacterial Phagosomes

Shintaro Seto[1], Kunio Tsujimura[1] and Yukio Koide[1,2,*]

[1] *Department of Infectious Diseases, 1-20-1 Handa-yama, Higashi-ku, Hamamatsu 431-3192, Japan*
[2] *Executive director, Hamamatsu University School of Medicine, 1-20-1 Handa-yama, Higashi-ku, Hamamatsu 431-3192, Japan*
**Corresponding author: Yukio Koide, koidelb@hama-med.ac.jp*

***Mycobacterium tuberculosis* (*M. tb*) is an intracellular pathogen that can replicate within infected macrophages. The ability of *M. tb* to arrest phagosome maturation is believed to facilitate its intracellular multiplication. Rab GTPases regulate membrane trafficking, but details of how Rab GTPases regulate phagosome maturation and how *M. tb* modulates their localization during inhibiting phagolysosome biogenesis remain elusive. We compared the localization of 42 distinct Rab GTPases to phagosomes containing either *Staphylococcus aureus* or *M. tb*. The phagosomes containing *S. aureus* were associated with 22 Rab GTPases, but only 5 of these showed similar localization kinetics as the phagosomes containing *M. tb*. The Rab GTPases responsible for phagosome maturation, phagosomal acidification and recruitment of cathepsin D were examined in macrophages expressing the dominant-negative form of each Rab GTPase. LysoTracker staining and immunofluorescence microscopy revealed that Rab7, Rab20 and Rab39 regulated phagosomal acidification and Rab7, Rab20, Rab22b, Rab32, Rab34, Rab38 and Rab43 controlled the recruitment of cathepsin D to the phagosome. These results suggest that phagosome maturation is achieved by a series of interactions between Rab GTPases and phagosomes and that differential recruitment of these Rab GTPases, except for Rab22b and Rab43, to *M. tb*-containing phagosomes is involved in arresting phagosome maturation and inhibiting phagolysosome biogenesis.**

Key words: acidification, cathepsin D, macrophage, membrane trafficking, *Mycobacterium tuberculosis*, phagolysosome biogenesis, phagosome maturation, Rab GTPase

Received 25 May 2010, revised and accepted for publication 19 January 2011, uncorrected manuscript published online 21 January 2011, published online 21 February 2011

Phagocytosis of pathogens by macrophages is an important process of the innate immune response. Pathogens are enveloped by phagocytic membranes to form phagosomes immediately following internalization. The phagosomes are then processed by a series of interactions with endosomes, resulting in phagosome maturation. During phagosome maturation, phagosomes fuse with lysosomes, in a process known as phagolysosome biogenesis, and acquire degradative and microbicidal properties. Several proteins, including the Rab GTPases, play pivotal roles in phagosome maturation and phagolysosome biogenesis (1). Rab5 is associated with phagosomes immediately after phagocytosis and facilitates the recruitment of Rab5 effector proteins, EEA1 and class III phosphatidylinositol-3-phosphate kinase (2). Membrane bound Rab5 is rapidly dissociated from the phagosome after its activation (3). Rab7 appears on the phagosome membrane after Rab5 dissociation and resides on the membrane during phagosome maturation (4). After acquisition of Rab7, phagolysosome biogenesis is accelerated by the recruitment of Rab7-interacting-lysosomal-protein (RILP) to the phagosome (5).

Mycobacterium tuberculosis (*M. tb*) is the causative agent of tuberculosis and has the ability to survive and proliferate in macrophages. Blockage of phagolysosome biogenesis may assist *M. tb* multiplication within infected macrophages (6,7). *M. tb* inhibits the acidification of phagosomes and recruitment of lysosomal hydratases to phagosomes, resulting in avoidance of the degradative and microbicidal properties of phagosomes (8). It has been thought that *M. tb* arrests phagosome maturation at the stage of Rab5–Rab7 conversion (9) on the mycobacterial phagosomes (10,11), because Rab7 was reported to be absent on mycobacterial phagosomes in macrophages (12–15). Sun et al. (16), however, demonstrated Rab7 localization on mycobacterial phagosomes. We have demonstrated that Rab7 is transiently recruited to and subsequently released from *M. tb*-containing phagosomes and that the release of Rab7 limits the recruitment of cathepsin D and RILP (17,18). Other Rab GTPases, Rab14 and Rab22a, were also demonstrated to be involved in the maturation arrest of *M. tb*-containing phagosomes (12,19), suggesting that *M. tb* disturbs the activity of some Rab GTPases regulating phagosome maturation and survives within macrophages.

Rab GTPases are encoded by a family of more than 60 genes and regulate membrane trafficking (20,21). The role of Rab GTPases in the trafficking of endocytosis and exocytosis has been well studied and their function in phagocytosis is being elucidated. Proteomic analysis revealed that several Rab GTPases are recruited to the latex bead-containing phagosomes (22–24). Smith et al. (25) investigated the interaction of a large number of Rab GTPases with phagosomes containing *Salmonella* in HeLa cells. However, there is currently insufficient information about the role of Rab GTPases in professional phagocytotic cells to understand how *M. tb* subverts membrane trafficking to survive within infected macrophages. In this study, we investigated the localization and function of 42 Rab GTPases in macrophages infected with *S. aureus* and *M. tb* during the progression of phagosome maturation. Through this comprehensive study, we demonstrate that the progression of phagosome maturation is achieved by the association of several Rab GTPases with the phagosome, leading to phagolysosome biogenesis, and that the release and/or dissociation of these Rab GTPases from *M. tb*-containing phagosomes has the relevance to *M. tb*-induced inhibition of phagolysosome biogenesis.

Results

Maturation of S. aureus*- and* M. tb*-containing phagosomes*

We have previously demonstrated that Rab7 controls the recruitment of the major lysosomal hydratase, cathepsin D, to the latex bead-containing phagosomes and that Rab7 is transiently recruited to and subsequently released from *M. tb*-containing phagosomes, suggesting that *M. tb* alters the localization of Rab7 to arrest phagosome maturation (17). In this study, we examined the localization of other Rab GTPases on *M. tb*-containing phagosomes in order to identify those with pivotal roles in phagosome maturation that are affected by the virulent *M. tb*. Raw264.7 macrophages were infected with *S. aureus* or *M. tb* and phagosomal maturation was compared. We confirmed acidification of the phagosomes and the recruitment of cathepsin D to the phagosomes in macrophages infected with *S. aureus* (Figure 1A,B). Both events, however, were inhibited in the macrophages infected with the virulent strain of *M. tb*, strain H37Rv (Figure 1C,D). We also found that the viability of *S. aureus* phagocytosed by macrophages quickly decreased, while *M. tb* was more robust, demonstrating survival and proliferation (Figure 1E). These results indicate that the maturation of the phagosomes containing *M. tb* was inhibited and that *M. tb* proliferated within Raw264.7 macrophages.

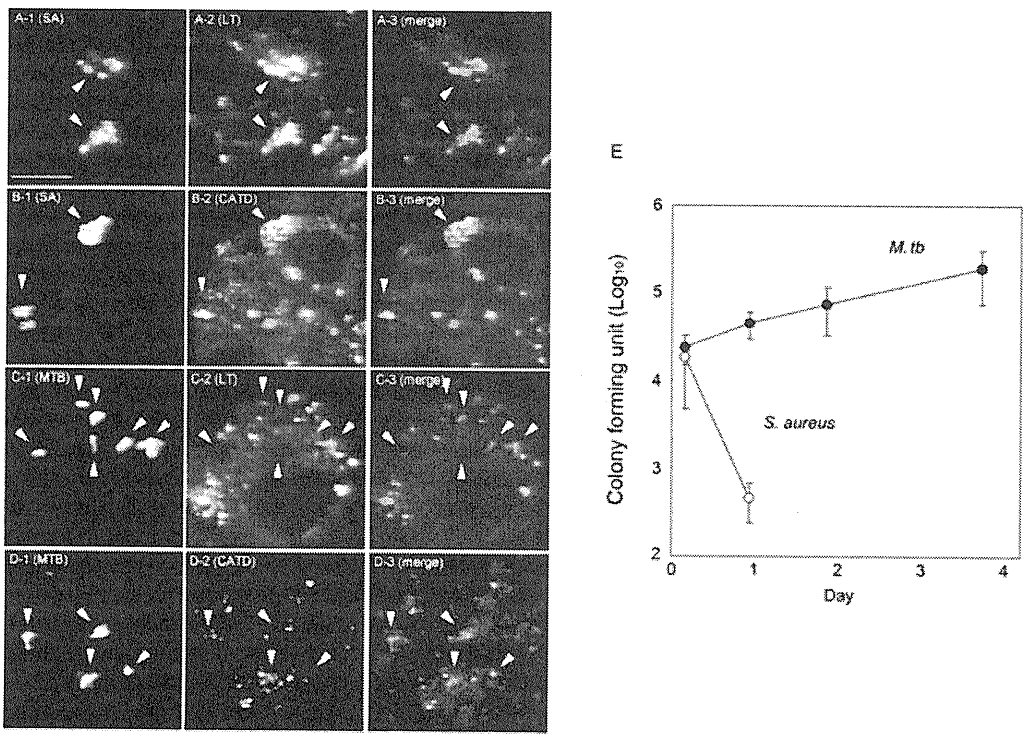

Figure 1: Maturation of phagosomes containing *S. aureus* and *M. tb*. A-D) Acidification and cathepsin D recruitment to phagosomes containing *S. aureus* and *M. tb* were examined. Raw264.7 macrophages were infected with Alexa405-labeled *S. aureus* (A and B) or *M. tb* (C and D) for 6 h. Infected cells were stained with LysoTracker (A and C) or anti-cathepsin D and Alexa488-labeled secondary antibodies (B and D), followed by observation with LSCM. A-1, B-1, C-1 and D-1 show *S. aureus* (SA) or *M. tb* (MTB). A-2, B-2, C-2 and D-2 show localization of LysoTracker (LT) or cathepsin D (CATD). A-3, B-3, C-3 and D-3 show merged images of macrophages and bacteria (merge). Arrows indicate the phagosomes containing SA or MTB. Scale bar, 10 μm. E) Intracellular growth of *S. aureus* and *M. tb* in macrophages. Raw264.7 macrophages (1×10^5 cells) were infected with *M. tb* for 4 h or *S. aureus* for 1 h at an MOI of 10. Infected cells were washed with DMEM three times to remove non-phagocytosed bacteria and then incubated with DMEM containing 10% FBS and 10 μg/mL gentamicin. Infected cells were collected at the indicated days and the number of viable bacteria was determined by a colony forming unit (CFU) counting assay. Data represent the means and standard deviations of three independent experiments. The CFU of *S. aureus* after day 2 was not plotted as they were less than 10.

Localization of Rab GTPases on S. aureus*-containing phagosomes*

To investigate the association of Rab GTPases with *S. aureus* phagosomes, Raw264.7 macrophages were transfected with the expression plasmid for enhanced green fluorescent protein (EGFP)-fused Rab GTPases and were then infected with *S. aureus* labeled with Texas Red. Infected cells were fixed and observed by laser scanning confocal microscopy (LSCM) at the indicated times up to 6 h. More than 100 internalized bacteria within macrophages expressing EGFP-fused Rab GTPase were examined at each time-point. The bacteria surrounded by EGFP signals were regarded as positive phagosomes associated with Rab GTPases. We investigated the kinetics of 42 distinct Rab GTPases whose expression was confirmed in Raw264.7 by reverse transcription-polymerase chain reaction (RT-PCR; data not shown). Their localization is summarized in Table S1 (Supporting information). We found 22 Rab GTPases associated with the phagosomes containing *S. aureus* (Figures 2 and S1). Localization of Rab GTPase could be classified into two types according to their kinetics on *S. aureus*-containing phagosomes, i.e. (i) transient localization or (ii) accumulation.

Figure 2A shows the localization kinetics of Rab GTPases exhibiting type I profiles. Rab5 and Rab22b were recruited to 30 and 90% of the phagosomes at 10 min post-infection (p.i.), respectively. Subsequently, these two Rab GTPases quickly disappeared from the phagosomes. Rab8, Rab8b, Rab11, Rab11b, Rab13, Rab14, Rab20, Rab22a, Rab32, Rab38 and Rab43 also showed transient phagosomal localization, peaking at 30 min and/or 1 h p.i. Figure 2B shows the localization kinetics of Rab GTPases exhibiting type II profiles. Rab7 localized on 40% of the phagosomes at 10 min p.i. The proportion of Rab7-positive phagosomes reached more than 80% at 30 min p.i. and remained at this level at 6 h p.i. as described previously (5,17). Localization of Rab7b, Rab9, Rab9b, Rab34 and Rab39 demonstrated similar kinetics to Rab7 localization. Rab27 and Rab37 did not localize to the phagosomes at the early stage of phagosome maturation. The proportions of Rab27- and Rab37-positive phagosomes increased only after 1 h p.i., suggesting that these Rab GTPases localize on the phagosome at the late stage of phagosome maturation. Rab23 localized on more than 80% of the phagosomes at all time-points investigated. The other 20 Rab GTPases investigated showed no significant associations with the phagosomes (less than 20% of the phagosomes) at all time-points up to 6 h (Figure S2). These results suggest that the network of Rab GTPases regulates the process of phagosome maturation at various time-points.

Localization of Rab GTPases on M. tb*-containing phagosomes*

We next investigated the localization of Rab GTPases on the phagosomes in macrophages infected with the virulent strain of *M. tb*. To investigate the association of Rab GTPases with *M. tb*-containing phagosomes, we infected Raw264.7 macrophages expressing EGFP-fused Rab GTPases with *M. tb* strain H37Rv expressing DsRed (Figure 2 and S1). The localization of Rab GTPases on *M. tb*-containing phagosomes was then examined as described above. Surprisingly, only five of the 22 Rab GTPases (Rab8, Rab8b, Rab9, Rab22b and Rab43) that localized on *S. aureus*-containing phagosomes showed the same localization kinetics on *M. tb*-containing phagosomes. According to the kinetics of localization on *M. tb*-containing phagosomes, the other 17 Rab GTPases were classified into three groups, showing: (i) transient association in contrast to the accumulation on *S. aureus*-containing phagosomes (Rab7, Rab9b, Rab23 and Rab34), (ii) similar kinetics but a lower rate of association than with *S. aureus*-containing phagosomes (Rab7b, Rab14, Rab22a, Rab32, Rab38 and Rab39) and (iii) a very low rate of association (Rab5, Rab11, Rab11b, Rab13, Rab20, Rab27 and Rab37).

Rab7 localized on 40% of *M. tb*-containing phagosomes at 10 min p.i., and the proportion of Rab7-positive *M. tb*-containing phagosomes increased to 80% at 30 min p.i., in a similar way to *S. aureus*-containing phagosomes. The proportion of Rab7-positive *M. tb*-containing phagosomes decreased after 1 h p.i. and reached 30% at 6 h p.i., while the proportion of Rab7-positive *S. aureus*-containing phagosomes remained at 80% up to 6 h p.i., confirming the previous results (17). Similar localization kinetics on *M. tb*-containing phagosomes were observed for Rab9b, Rab23 and Rab34 (type I). Rab7b localized to 40% of *M. tb*-containing phagosomes, as was seen with *S. aureus*-containing phagosomes. Rab7b-positive phagosomes containing *S. aureus* increased to more than 80% up to 6 h p.i., but the proportion of Rab7b-positive phagosomes containing *M. tb* did not change. Rab14, Rab22a, Rab32, Rab38 and Rab39 also showed a weaker association with *M. tb*-containing phagosomes compared with *S. aureus*-containing phagosomes (type II). Rab5 localized on 30% of *S. aureus*-containing phagosomes at 10 min p.i., but the proportion of Rab5-positive *M. tb*-containing phagosomes was less than 20%. Rab11 localized on 80% of *S. aureus*-containing phagosomes at 30 min p.i., but showed no significant association on *M. tb*-containing phagosomes (less than 20%). Rab11b, Rab13, Rab20, Rab27 and Rab37 also showed no significant association with *M. tb*-containing phagosomes (type III). These results suggest that the dissociation of 17 Rab GTPases might disrupt membrane trafficking in the maturation process of *M. tb*-containing phagosomes. We found that 20 Rab GTPases, which were not associated with *S. aureus*-containing phagosomes, also showed no significant association with *M. tb*-containing phagosomes (Figure S2).

Localization of Rab GTPases on isolated phagosomal fractions

To examine the recruitment of endogenous Rab GTPases to the phagosomes, we conducted immunoblotting analysis to detect Rab GTPases in isolated phagosomes containing latex beads and *M. tb*. Raw264.7 macrophages were allowed to phagocytose latex beads or infected with